Published online 30 April 2018

Nucleic Acids Research, 2018, Vol. 46, No. 11 ***5525–5546***
doi: 10.1093/nar/gky265

StpA and Hha stimulate pausing by RNA polymerase by promoting DNA–DNA bridging of H-NS filaments

Beth A. Boudreau[1], Daniel R. Hron[1], Liang Qin[2], Ramon A. van der Valk[2], Matthew V. Kotlajich[1], Remus T. Dame[2] and Robert Landick[1,3,*]

[1]Department of Biochemistry, University of Wisconsin–Madison, Madison, WI 53706, USA, [2]Leiden Institute of Chemistry, Leiden University, Einsteinweg 55, 2333 CC, Leiden, Netherlands and [3]Department of Bacteriology, University of Wisconsin–Madison, Madison, WI 53706, USA

Received December 22, 2017; Revised March 12, 2018; Editorial Decision March 27, 2018; Accepted April 03, 2018

ABSTRACT

In enterobacteria, AT-rich horizontally acquired genes, including virulence genes, are silenced through the actions of at least three nucleoid-associated proteins (NAPs): H-NS, StpA and Hha. These proteins form gene-silencing nucleoprotein filaments through direct DNA binding by H-NS and StpA homodimers or heterodimers. Both linear and bridged filaments, in which NAPs bind one or two DNA segments, respectively, have been observed. Hha can interact with H-NS or StpA filaments, but itself lacks a DNA-binding domain. Filaments composed of H-NS alone can inhibit transcription initiation and, in the bridged conformation, slow elongating RNA polymerase (RNAP) by promoting backtracking at pause sites. How the other NAPs modulate these effects of H-NS is unknown, despite evidence that they help regulate subsets of silenced genes *in vivo* (e.g. in pathogenicity islands). Here we report that Hha and StpA greatly enhance H-NS-stimulated pausing by RNAP at 20°C. StpA:H-NS or StpA-only filaments also stimulate pausing at 37°C, a temperature at which Hha:H-NS or H-NS-only filaments have much less effect. In addition, we report that both Hha and StpA greatly stimulate DNA–DNA bridging by H-NS filaments. Together, these observations indicate that Hha and StpA can affect H-NS-mediated gene regulation by stimulating bridging of H-NS/DNA filaments.

INTRODUCTION

Horizontal gene transfer contributes crucially to bacterial genetic diversity by allowing the transfer of genetic material from one organism to another (1). To suppress uncontrolled expression of these new genes, which can compromise cell viability, enterobacteria express H-NS-family nucleoid-associated proteins (NAPs) that bind and silence horizontally acquired DNA based on its higher AT-content through formation of nucleoprotein filaments (2–5 and reviewed in Ref. 6). In some cases, specific regulatory mechanisms that overcome silencing evolved subsequently to leverage the new genetic potential (7).

In *Escherichia coli*, H-NS (histone-like nucleoid structuring) is a 15.5 kDa protein. H-NS forms dimers at low concentrations, which assemble into larger multimers at higher concentrations (8,9). Some α-, some β- and most γ-proteobacteria retain at least one copy of H-NS; pathogenic species often encode one or more additional H-NS paralogs (10–12). The best studied among the H-NS paralogs is StpA (suppressor of *td* phenotype A; Ref. 13). *E. coli* StpA is 15.3 kDa in size. StpA is believed to exist predominantly as a heterodimer in association with H-NS *in vivo* (14), because it is degraded by the Lon protease if not bound to H-NS (15). H-NS is also bound and modulated by proteins from the YmoA family of proteins (16). Similar to the H-NS paralogs, these proteins are found in commensal Gram-negative strains but are more abundant in pathogenic strains (11). Hha (high hemolysin activity) is a YmoA family protein expressed in *E. coli* that can modulate H-NS filament activities. Hha is 8 kDa in size and can associate with both H-NS and StpA (17,18). *E. coli* K-12 also encodes a paralog of Hha, YdgT (19). Although it lacks a separate DNA-binding domain (DBD) present in H-NS and StpA, Hha regulates many genes in association with H-NS (Figure 1A and B; Refs. 17,20,21), and may affect others independently of H-NS (22).

H-NS, aided by its paralogs and modulators (4,23), forms nucleoprotein filaments (Figure 1C) that silence genes in *E. coli* by affecting all stages of transcription: initiation, elongation and termination. H-NS and StpA filaments inhibit initiation by blocking binding of RNA polymerase (RNAP) to promoters (24–28) and by blocking promoter escape (29–31). Bridged H-NS filaments also can prevent RNAP elongation into silenced genes by stimulating pausing and subsequent Rho-dependent termination at a subset of sites prone

*To whom correspondence should be addressed. Tel: +1 608 265 8475; Email: landick@bact.wisc.edu

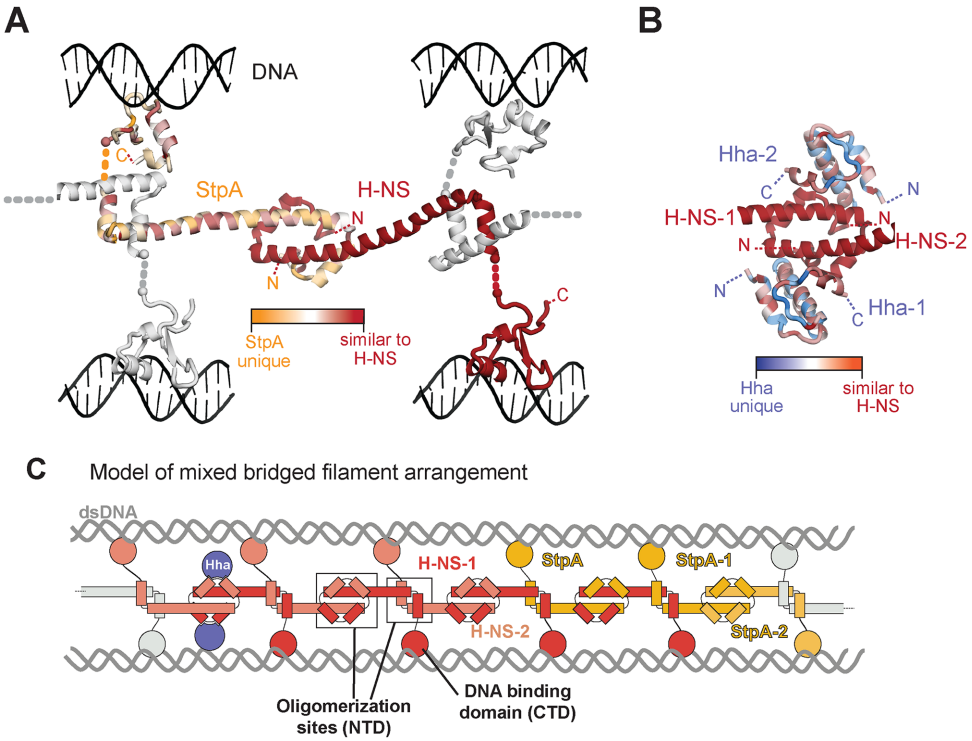

Figure 1. Structures and sequence similarities of H-NS, StpA and Hha. (**A**) StpA (orange/pink) modeled into the H-NS (red) head–head, tail–tail filament structure of the H-NS NTD (PDB ID: 3NR7; Ref. 57). Models of the StpA and H-NS CTDs interacting with DNA (DNA binding domain, DBD) are positioned to represent contacts in a bridged nucleoprotein filament based on an H-NS CTD structure (PDB ID: 1HNR; Ref. 99) and the H-NS paralog Ler CTD bound to DNA (PDB ID: 2LEV; Ref. 100). The StpA sequence conservation is shown as a color gradient of unique to StpA (orange) to similar to H-NS (red). StpA sequences from 26 species were aligned with H-NS to identify unique StpA residues and compared to H-NS to calculate sequence conservation (Supplementary Figure S1A and B). N and C indicate the N-terminus and C-terminus of proteins, respectively. (**B**) Hha sequence similarity compared to H-NS NTD is indicated by color gradient from *red* (similar to H-NS) to *blue* (unique to Hha) on both Hha monomers (Hha-1 and Hha-2) in the Hha:H-NS complex structure (PDB ID: 4ICG; Ref. 17). Although Hha is a member of the distinct YmoA protein family, it retains sequence similarity to H-NS. Hha sequences from 41 species were aligned with H-NS residues 1–83 to identify unique Hha residues (Supplementary Figure S1C). (**C**) Schematic adapted from Ref. (17) of the proposed arrangement of H-NS, StpA and Hha in a bridged nucleoprotein filament (H-NS, red and pink; StpA, yellow and pale yellow; Hha, blue; dsDNA, gray). The arrangement of H-NS, StpA and Hha in mixed nucleoprotein filaments is unknown.

to RNAP backtracking, but not at non-backtracked sites called elemental pause sites (5,32–34). The NusG paralog RfaH, which inhibits pausing, and the transcript cleavage factor GreB, which rescues backtracked RNAP, counteract H-NS-mediated silencing and H-NS-stimulated pausing (32,35,36). Temperature, osmolarity and pH also affect H-NS (37–39) and modulate the ability of H-NS to inhibit transcription (32) by mechanisms that remain poorly understood.

H-NS-mediated gene silencing has been investigated at many *E. coli* operons, notably the *bglGFB* and *hlyCABD* operons. The cryptic *bgl* operon, which encodes proteins responsible for β-glucoside utilization, is silenced in *E. coli* K-12 by H-NS and StpA filaments that nucleate at upstream and downstream regulatory elements (URE and DRE) and block promoter function (40–42). Additionally, the H-NS filament can prevent elongation and enhance termination of RNAPs initiated at a *bgl* antisense promoter just downstream from the DRE (5,32). The *bgl* operon is thus a model system to elucidate how H-NS-modulated filaments affect elongating RNAP. The *hlyCABD* operon, present in pathogenic *E. coli*, encodes production of hemolysin, which lyses red blood cells. Expression of *hlyCABD* is repressed by a nucleoprotein filament containing Hha and H-NS, which prevents full-length transcript formation (20,37). Binding of RfaH to transcription complexes and environmental factors, like temperature, allow for expression of the operon despite filament formation (35,43,44). The interplay of H-NS, H-NS modulators and environmental and elongation factors make the *hly* operon another model system for study of the effects of H-NS filaments on transcription elongation.

E. coli grown in rich medium (Luria broth) at 37°C contains ∼47 000 copies of H-NS/cell, ∼5 200 copies of StpA/cell, ∼240 copies of Hha/cell and ∼200 copies of YdgT/cell during exponential phase (45–47), but these numbers change with growth condition (48–50). ChIP experiments show that H-NS and StpA can bind the same DNA loci covering ∼17% of the *E. coli* genome in discrete DNA segments (51–54) with segment lengths that average ∼2 kb and range from 0.5–50 kb (51,52). Given the cellular concentration of StpA, these nucleoprotein filaments must contain more H-NS:H-NS dimers than StpA:H-NS heterodimers on average. However, the distribution of StpA within filaments is poorly defined and could be driven by DNA sequence specificity (55). Hha is associated with H-NS filaments *in vivo* (17,18,21), but the distribution of Hha

and YdgT among H-NS filaments is uncertain. The genomic distribution of H-NS is similar in exponential and stationary phase (52), but it is unclear whether the distribution of StpA, Hha or YdgT among filaments changes with growth phase or environment.

Some properties of H-NS-family filaments have been characterized *in vitro*. H-NS contains an N-terminal oligomerization domain (NTD) and a C-terminal DBD connected by a flexible linker (Figure 1C); both domains and the linker are required for nucleoprotein filament formation (Figure 1C; Refs. 56–58). At high (>5 mM) Mg^{2+} (39,59) or at low (≤66 DBD/kb) monomer-to-DNA ratio (32), H-NS filaments can preferentially form bridged filaments in which the alternating DBDs contact different double-stranded DNA segments (Figure 1C). These bridging interactions bring DNA duplexes together into a proposed superhelical filament in which the H-NS filament bridges the two DNAs (57). Linear filaments are observed in conditions that do not favor DNA bridging, such as at low (<5 mM) Mg^{2+} (59) or high monomer-to-DNA ratio (≥200 DBD/kb; Refs. 32,60). In the formation of linear filaments, H-NS binds to DNA and oligomerizes contiguously along one segment of a single DNA duplex to form a linear filament (sometimes called a 'stiffened' filament, Refs. 59,60). Not surprisingly given its sequence similarity, StpA behaves in a similar manner to H-NS (Figure 1A and C). StpA filaments adopt either a bridged conformation in the absence of Mg^{2+}, or, in 10 mM Mg^{2+}, a different structure in which multiple DNA segments appear to be compacted (26,61). Hha, which interacts with the NTD of H-NS or StpA (Figure 1B and C; Refs. 17,18), increases DNA binding affinity of H-NS, and promotes DNA bridging, including multi-segment bridging, even in the absence of Mg^{2+} (17,39,62). Despite strong evidence of interactions among H-NS-family proteins, little is known about the properties and roles of the mixed filaments (53,54,63).

To gain insight into the effects of H-NS paralogs and modulators on transcribing RNAP, we selected one model paralog, StpA, and one model modulator, Hha. Using a combination of *in vitro* biochemical and biophysical assays, we characterized H-NS filaments formed with Hha or StpA and compared their effects on elongating RNAP using a previously developed *in vitro* transcription assay (32). Our results provide a biochemical framework in which insight is gained into how mixed H-NS filaments affect gene regulation.

MATERIALS AND METHODS

Materials

Reagents were obtained from ThermoFisher (Waltham, MA, USA) or Sigma-Aldrich (St. Louis, MO, USA), unless otherwise specified. Oligonucleotides for DNA construction (Supplementary Table S1) were obtained from IDT (Coralville, IA, USA); ribonucleotide triphosphates (rNTPs), from Promega (Madison, WI, USA); [α-^{32}P]GTP and [γ-^{32}P]ATP, from Perkin Elmer (Waltham, MA, USA); polyethyleneimine (PEI, avg. MW = 60 000), from Acros Organics; and DNA-modifying enzymes, from New England Biolabs (Ipswich, MA, USA).

Plasmid construction

Plasmids used for protein expression and *in vitro* transcription template preparation are described in Supplementary Table S2 and were confirmed by DNA sequencing.

To overexpress StpA with a C-terminal His_6 tag, the *stpA* coding sequence (CDS) was amplified from MG1655 genomic DNA with primers #8595 and #8488 (Supplementary Table S1). pET28A and the amplified *stpA* DNA were digested with BamHI and NcoI and ligated with T4 DNA ligase. The resulting plasmid contained *stpA* in-frame with a C-terminal TEV protease cleavage site and a His_6 tag (pHisStpA). A non-tagged StpA expression plasmid (pStpA) was constructed using Gibson assembly (64) to combine polymerase chain reaction (PCR) products of the pET21d backbone (amplified from pHisHNS with primers #11781 and #11782) and *stpA* (amplified from MG1655 genomic DNA with primers #11783 and #11784).

The Hha expression plasmid, pMBPHha, was generated by Gibson assembly. The *hha* CDS was amplified from MG1655 genomic DNA using primers #9627 and #9628 containing overhangs with overlap to pMAL-c5x (NEB). The pMAL-c5x backbone was amplified using primers #9623 and #9624 with overhangs containing sequence complementary to the *hha* amplicon. PCR-amplified DNA was then gel extracted and purified using a Qiagen gel extraction kit. Purified fragments were combined by Gibson assembly to generate pMBPHha, in which the MBP gene and the FactorXa cleavage site are expressed as a protein fusion on the N-terminus of Hha.

The pBB10 plasmid, containing the template DNA for transcription of *hlyC*, was constructed by amplifying the 5′ untranslated region, *hlyC*, and a portion of *hlyA* from pSF4000 (35,65) using primers #11052 and #11053. The *hlyC* PCR product and pMK110 were digested with SpeI. Digests were gel-purified and ligated with T4 DNA ligase. In the resulting pBB10 plasmid, the *hlyC* gene is downstream of the λP_R promoter and a C-less cassette (Figure 8).

The pBB20 plasmid, containing 500 bp of the *hlyC* gene upstream of the λP_R promoter inserted into the *bgl* template for *in vitro* transcription experiments, was generated by Gibson assembly (Figure 7). The *bgl* template plasmid (pMK110) was amplified with primers #11900 and #11901. The *hlyC* insert was amplified from pSF4000 using primers #11902 and #11903, which contain overhangs complementary to primers #11900 and #11901. PCR products were gel-purified using Qiagen gel purification kit and the subjected to Gibson assembly.

Protein purification

RNAP, σ^{70}, GreB and C-terminally 6× His-tagged H-NS were purified as previously described (32).

StpA purification. BL21 λDE3 cells transformed with pHisStpA were grown in 2 l of LB supplemented with kanamycin (50 μg/ml) at 37°C to an OD_{600} of ∼0.4. StpA expression was induced with 0.4 mM isopropyl β-D-1-thiogalactopyranoside (IPTG) for 4 h at 25°C. Cells were centrifuged at 3000 × *g* for 15 min at 4°C, and the cell pellet was resuspended in 30 ml lysis buffer (0.2 M NaCl,

20 mM Tris–HCl pH 7.5, 5% glycerol, 2 mM ethylenediaminetetraacetic acid (EDTA), 1 mM β-mercaptoethanol (β-ME), 1 mM dithiothreitol (DTT)) supplemented with phenylmethylsulfonyl fluoride (PMSF) and protease inhibitor cocktail (PIC; 31.2 mg benzamide/ml, 0.5 mg chymostatin/ml, 0.5 mg leupeptin/ml, 0.1 mg pepstatin/ml, 1 mg aprotonin/ml, 1 mg antipain/ml). Cells were lysed with 0.7 g lysozyme followed by sonication. The lysate was cleared by centrifugation at 11 000 × *g* for 15 min at 4°C. DNA-associated proteins were precipitated by addition of PEI to 0.6% (weight/volume) with gentle stirring. The precipitate was collected by centrifugation at 11 000 × *g* for 15 min at 4°C. The pellet was gently resuspended in PEI wash buffer (10 mM Tris–HCl pH 7.5, 0.1 mM EDTA, 5% glycerol, 0.2 M NaCl, 1 mM DTT) and then centrifuged at 11 000 × *g* for 15 min at 4°C. Subsequently, StpA was eluted by gently resuspending the pellet in PEI elution buffer (10 mM Tris-HCl pH 7.5, 0.1 mM EDTA, 5% glycerol, 0.8 M NaCl, 1 mM DTT) and the insoluble material was removed by centrifugation at 11 000 × *g* for 15 min at 4°C. StpA was precipitated with gentle stirring overnight after slow addition of finely ground ammonium sulfate to 0.37 g/ml (60% saturation). Precipitated StpA was collected by centrifugation at 27 000 × *g* for 15 min at 4°C. The pellet was resuspended in 35 ml nickel-binding buffer (20 mM Tris–HCl pH 7.5, 5 mM imidazole, 5 mM β-ME, 1 M NaCl). StpA was loaded at 2.5 ml/min onto a 5 ml HisTrap HP column attached to an AktaPrime (GE Healthcare) and washed with 30 ml of nickel-binding buffer. StpA was eluted over a 0–50% gradient of nickel-elution buffer (nickel-binding buffer containing 1 M imidazole) over 20 min at 2.5 ml/min. StpA eluted at ∼400 mM imidazole. Fractions containing StpA were pooled and dialyzed into nickel-binding buffer. The His_6 tag was cleaved off overnight at 4°C with the addition of TEV protease (16 μg TEV/1 mg StpA). The mixture was re-applied to the nickel column as described above. Untagged StpA was collected from the flow-through and dialyzed into storage buffer (20 mM Tri–HCl pH 7.5, 1 M KCl, 40% glycerol). Purity (∼90%) of the dialyzed protein was confirmed by sodium dodecyl sulphate-polyacrylamide gel electrophoresis (SDS-PAGE). StpA was concentrated to 300 μM and aliquoted for storage at −80°C.

Non-tagged StpA purification. StpA was purified as described in (61). Briefly, Δ*hns* BL21 λDE3 cells transformed with pStpA and pHiC (Supplementary Table S2) were grown in 2 L of LB supplemented with ampicillin (100 μg/ml) and gentamycin (10 μg/ml) at 37°C to an OD_{600} of ∼0.4. P1 transduction with lysate from JW1225-2 was used to generate a Δ*hns* BL21 λDE3 strain. StpA expression was induced by addition of 500 μM IPTG and 250 μg carbenicillin/ml for 16 h at 25°C. Cells were centrifuged at 3000 × *g* for 20 min at 4°C, and the cell pellet was resuspended in 30 ml lysis buffer (50 mM Tris–HCl pH 7.5, 2 mM EDTA, 5% glycerol, 0.2 M NaCl, 1 mM β-ME, 1 mM DTT) supplemented with PMSF and PIC. Cells were lysed by sonication and the lysate was cleared by centrifugation at 27 000 × *g* for 20 min at 4°C. PEI was slowly added to the lysate with gentle stirring to a final concentration of 0.3% to precipitate DNA-associated proteins. Precipitation was continued for 5 min at 4°C. The precipitate was pelleted by centrifugation at 11 000 × *g* for 15 min at 4°C. The pellet was resuspended in 30 ml PEI elution buffer (50 mM Tris–HCl pH 7.5, 0.1 mM EDTA, 5% glycerol, 0.5 M NaCl, 1 mM DTT) and centrifuged at 11 000 × *g* for 15 min at 4°C. The supernatant containing StpA was removed and StpA was then precipitated with gentle stirring overnight after slow addition of finely ground ammonium sulfate to 40% saturation. Precipitated protein was removed by centrifugation at 27 000 × *g* for 15 min at 4°C. The pellet was resuspended in 20 ml of 50 mM Tris–HCl, pH 7.5 and dialyzed against no-salt buffer (50 mM Tris–HCl pH 7.5, 1 mM EDTA, 10% glycerol, 0.5 mM DTT). Precipitated protein was separated by centrifugation at 27 000 × *g* for 15 min at 4°C. The StpA-containing pellet was resuspended in 25 mL of heparin binding buffer (50 mM Tris–HCl pH 7.5, 1 mM EDTA, 10% glycerol, 300 mM NaCl) and applied to a 5 ml HiTrap Heparin HP column (GE Life Sciences). StpA was eluted using a 6-column-volume gradient of 0.3–1 M NaCl in heparin binding buffer. StpA eluted at ∼0.8 M NaCl. StpA-containing fractions were pooled and dialyzed against 50 mM Tris–HCl, pH 7.5, 1 mM EDTA, 10% glycerol. Precipitated protein was pelleted at 8 000 × *g* for 10 min at 4°C and resuspended in storage buffer (50 mM Tris–HCl, pH 7.5, 1 mM EDTA, 10% glycerol, 0.5 mM DTT, 0.3 M NaCl). About 1 mg of StpA was purified to 95% purity as determined by SDS-PAGE and Coomassie staining. This protein was used for the DNA bridging pulldown assay (see below).

Non-tagged H-NS purification. BL21 λDE3 cells transformed with pHisHNS and pHiC (Supplementary Table S2) were grown in 2 L of LB in the presence of ampicillin (100 μg/ml) and gentamicin (10 μg/ml) at 37°C to an OD_{600} of ∼0.6 before inducing H-NS expression with 500 μM IPTG for 4 hours at 30°C in the presence of 0.25 mg carbencillin/ml. Induced cultures were pelleted at 3 000 × *g* for 15 min at 4°C. Cell pellets were resuspended in 30 ml lysis buffer (20 mM Tris–HCl pH 7.5, 0.1 M NaCl, 5% glycerol, 2 mM EDTA, 1 mM β-ME, 1 mM DTT) supplemented with PMSF and PIC and lysed by sonication. Insoluble material was removed by centrifugation at 11 000 × *g* for 15 min at 4°C. H-NS was precipitated by the slow addition of equilibrated PEI to 0.6% w/v. PEI (∼8% w/v) was equilibrated by dialyzing against lysis buffer without β-ME and DTT. After centrifugation, the PEI pellet was resuspended in 30 ml of PEI wash buffer (10 mM Tris–HCl pH 7.5, 0.1 mM EDTA, 5% glycerol, 1 mM DTT, 0.15 M NaCl) followed by centrifugation at 11 000 × *g* for 15 min at 4°C. H-NS was eluted by resuspending the pellet in 30 mL of PEI elution buffer (10 mM Tris–HCl pH 7.5, 0.1 mM EDTA, 5% glycerol, 1 mM DTT, 0.6 M NaCl). Insoluble material was pelleted at 11 000 × *g* for 15 min at 4°C. H-NS was precipitated overnight with gentle stirring by addition of finely ground ammonium sulfate to 0.37 g/ml (60% saturation). Precipitated H-NS was pelleted at 27 000 × *g* for 15 min at 4°C. The H-NS pellet was resuspended in 35 ml nickel-binding buffer. H-NS was applied to a 5 mL HisTrap Ni^{2+} column (GE Healthcare) and eluted with a gradient elution from 0–50% of nickel-binding buffer containing 1 M imidazole in 50 ml. Fractions containing H-NS were pooled and TEV protease was added to cleave off the 6×-His tag.

Cleaved H-NS was reapplied to the HisTrap Ni^{2+} column and the H-NS-containing flow through was collected. Removal of the His-tag was also confirmed by staining with InVision His stain (ThermoFisher). Non-tagged H-NS in nickel-binding buffer was diluted to 100 mM NaCl with addition of heparin-binding buffer (10 mM Tris–HCl pH 7.5, 0.2 M NaCl, 0.1 mM EDTA, 5% glycerol, 1 mM DTT) and applied to a 5 ml HiTrap Hep column (GE Healthcare). H-NS was eluted in heparin-elution buffer (10 mM Tris–HCl pH 7.5, 1 M NaCl, 0.1 mM EDTA, 5% glycerol, 1 mM DTT). Fractions containing H-NS were pooled, concentrated and dialyzed against storage buffer (20 mM Tris–HCl pH 7.5, 0.3 M KCl, 10% glycerol) and stored in aliquots at −80°C. Purity of H-NS (∼95%) was confirmed by SDS-PAGE and Coomassie staining.

Hha purification. BLR λDE3 cells containing pMBPHha (Supplementary Table S2) were grown at 37°C in 2 L of LB supplemented with 0.2% glucose and ampicillin (100 μg/ml) to an OD_{600} of ∼0.5 then were induced with 0.3 mM IPTG for 2 h at 37°C. Cells were spun at 3 000 × *g* for 15 min at 4°C then were resuspended in MBP buffer (20 mM Tris–HCl, pH7.5, 200 mM NaCl, 1 mM EDTA, 1 mM DTT) containing PMSF and PIC. Cells were lysed by sonication and the lysate was cleared by centrifugation at 20 000 × *g* for 20 min at 4°C. The lysate was applied to a 5 ml amylose column (GE Healthcare) and then eluted by block elution with MBP buffer containing 10 mM maltose. Fractions containing MBP-Hha were pooled and dialyzed into cleavage buffer (20 mM Tris–HCl, pH 8.0, 100 mM NaCl, 2 mM $CaCl_2$). MBP was removed from Hha by incubation with 1 μg Factor Xa (NEB) for every 1.8 mg fusion protein for 8 h at 4°C. Cleaved Hha was dialyzed into storage buffer (25 mM HEPES-KOH, pH 8.0, 150 mM NaCl, 1 mM DTT, 5% glycerol) and loaded onto a size-exclusion Superdex 75 prep grade 16/60 column (GE Healthcare). Fractions containing Hha were concentrated and stored at −80°C. SDS-PAGE and Coomassie staining confirmed that ∼2 mg of Hha was purified to ∼95% purity.

DNA template purification for *in vitro* transcription and AFM

Templates for *in vitro* transcription were generated as described previously (32). Briefly, template DNA was amplified with OneTaq DNA polymerase from primers #3071 and #645 on pMK110, pBB10 or pBB20 for the *bgl* template, *hlyC* template or *upstream* template, respectively. The PCR product was gel purified and electroeluted. The template was further purified by phenol extraction and ethanol precipitation before resuspending in 15 mM HEPES–KOH, pH 8.0. Templates for atomic force microscopy (AFM) were made using the same PCR amplification and gel purification protocol, but were then purified further using a Gene Clean Kit (MPBio, Santa Ana, CA, USA). The purity and concentration of the final product was assessed by agarose gel electrophoresis followed by ethidium bromide staining and by absorbance at 260 nm (Nanodrop; ThermoFisher).

In vitro transcription

Transcription assays using the *bgl, upstream* and *hlyC* templates were performed as described previously (B.A. Boudreau, *et al.,* submitted for publication in Methods in Molecular Biology and Ref. 32). To form wild-type *E. coli* RNAP σ^{70} holoenzyme, 2-fold molar excess of σ^{70} was incubated with core RNAP (β, β′, α, α, ω subunits) in RNAP storage buffer (20 mM Tris–HCl pH 7.9, 0.1 mM EDTA, 0.1 M NaCl, 10 mM $MgCl_2$, 1 mM DTT, 40% glycerol) for 30 min at 30°C. Halted elongation complexes (ECs) were formed by incubating 150 nM holoenzyme with 100 nM template DNA containing the λP_R promoter and 26 nt C-less cassette in electrophoretic mobility shift assay (EMSA) buffer (40 mM HEPES-KOH pH 8.0, 100 mM potassium glutamate, 8 mM magnesium aspartate, 0.022% NP-40, 100 μg acetylated bovine serum albumin (BSA)/ml, 10% glycerol) supplemented with 1 mM DTT, 150 μM ApU, 10 μM adenosine triphosphate (ATP) and uridine triphosphate (UTP), 2.5 μM guanosine triphosphate (GTP), and 20 μCi [α-^{32}P]GTP at 37°C for 15 min. In the absence of cytosine triphosphate (CTP), RNAP stops after synthesizing a 26-nt RNA transcript (A26 ECs), where the 3′-end of the RNA is adenosine and the next nucleotide to be added is CMP. The A26 ECs were diluted to 10 nM with various combinations of NAPs (H-NS, StpA, Stpa:H-NS or Hha:H-NS) at different protein/kb ratios (see figure legends), in EMSA buffer containing 40 U RNasin/μl (Promega, Madison, WI), 0.1 mg rifampicin/ml, and 0.5 mM DTT and incubated at 20°C for 20 min to form filaments downstream of the EC. After filaments were formed on A26 ECs, a sample of each reaction was separated by 3% native PAGE (described below) alongside filaments formed on non-EC-containing DNA to confirm filament formation.

Elongation was restarted by addition of all 4 NTPs to 30 μM each and subsequent time points were taken by adding 7 μl of the elongation mix to 193 μl of stop solution (15 mM EDTA, 1.5 μl glycogen, 100 μl TE-equilibrated phenol, pH 7.9). RNA was phenol extracted and ethanol precipitated. Precipitated RNA was resuspended in formamide stop dye (95% formamide, 20 mM EDTA, 0.05% bromophenol blue, 0.05% xylene cyanol) to 100–200 counts/μl. RNA products were separated on 12 and 6% urea-PAGE alongside [γ-^{32}P]ATP end-labeled MspI-digested pBR322 and HaeIII-digested phiX174 markers. Gels were exposed to a PhosphorImager screen, and the screen was scanned using Typhoon PhosphorImager software and quantified in ImageQuant version 5.2 (GE Lifesciences). Gel images were adjusted for brightness and contrast without loss of data.

In some experiments (Figures 4 and 8), elongation was restarted by addition of 1 mM of each NTP (4 mM total). Because excess NTP can chelate free magnesium, 12 mM magnesium aspartate, rather than 8 mM magnesium aspartate, was added to the reaction to keep the free magnesium concentration constant in all experiments. For elongation in the presence of GreB (Figure 4), 50 nM GreB (diluted in 3× EMSA buffer) was added to the elongation mixes during filament formation. Transcription on the *hlyC* template (Figure 8) was carried out at both 20 and 37°C using a fraction of the same elongation mixture containing either H-

NS, StpA, StpA:H-NS or Hha:H-NS and in the presence of 1 mM NTPs.

Imaging and analysis of paused RNA transcripts

RNA products were imaged and quantified as described above. Lines (6-pixel wide) were drawn for each gel lane (aligned to the center for the entire length in which signal was present) and converted to average signal intensity at each position along the axis of electrophoresis. The signal intensities were normalized so the total signal in each lane was the same. Using end-labeled markers (MspI-digested pBR322 and HaeIII-digested ϕX174 DNA; NEB) run alongside, each position along the electrophoretic axis was converted to a nucleotide length using a multi-factor polynomial function fit to fragment length versus pixel along the electrophoretic axis (KaleidaGraph; Synergy Software). RNA on a 6% gel fit to a 6-factor function whereas on a 12% gel, a combination of 6- and 4-factor polynomial functions were used for the long and short products, respectively. Signal from each sample was then plotted as a function of approximate RNA length to create pseudo-densitometry profiles (RNA lengths are based on single-stranded DNA electrophoretic mobility and thus are not exact). The mean transcript length (MTL) was calculated as the sum of the products of the signal and RNA length for each position along the line divided by the total RNA signal, $(\Sigma(\text{signal}*\text{RNA length})_n)/\Sigma(\text{signal})_n$.

To generate a graphic indication of the distribution RNA lengths in a given sample, transcript lengths that constituted 30% of the total transcripts surrounding the MTL (15% in the longer direction and 15% in the shorter direction) were calculated and plotted as gradients centered on the MTL. Comparing these MTLs and distributions gives a useful visual representation of how each filament impacts overall elongation averaged over all pause sites.

The percent of the G35 pause was calculated using ImageQuant lines (6-pixel wide) to determine the total signal from the entire sample and the signal between the A26 and G35 RNA products. The area under the curve for RNAs between A26 and G35 was calculated using the multipeak fitting package in IgorPro (Wave Metrics). The percent of the G35 pause was calculated as the G35 signal divided by the total signal. Pause strength was determined for select pauses as described in (66).

Electrophoretic mobility shift assay (EMSA)

EMSAs were performed as previously described (32) with minor modifications. DNA (100 nM) was end-labeled with [γ-^{32}P]ATP with T4 polynucleotide kinase (PNK) at 37°C for 30 min. PNK was inactivated by incubation at 65°C for 15 min before using the labeled DNA. [γ-^{32}P]ATP-labeled DNA template (10 nM) was incubated with StpA, H-NS, StpA:H-NS or Hha:H-NS at different concentrations in EMSA buffer at 20°C for 20 min to form filaments. Working protein stocks were always diluted in 3× EMSA buffer. Samples were then loaded on a 3% native polyacrylamide gel (29:1 acrylamide:bisacrylamide) in 0.5× tris-borate EDTA (TBE) and electrophoresed at 250V for 5 h at 4°C. The gels were dried and imaged using a Typhoon Phosphorimager.

Atomic force microscopy (AFM)

AFM samples were prepared as described with some modifications (32,67). Aminopropyl silatrane (APS) was synthesized and stored as described (67). Briefly, freshly cleaved mica was incubated with 100 or 170 μM APS for 30 min at room temperature, washed with Milli-Q purified (MQ) H_2O, dried with Argon (Ar) and cured overnight in Ar under reduced pressure. Filaments to be imaged by AFM were prepared by incubating proteins and *bgl* DNA (purified as described above) in AFM buffer (40 mM HEPES-KOH pH 8.0, 100 mM potassium glutamate, 8 mM magnesium aspartate) at 20°C for 20 min. A sample of filaments was separated on a native gel as a control (data not shown) before filaments were applied to the mica surface. Filaments were absorbed onto the APS-mica surface either undiluted or at a 1:10 dilution at 4°C or at room temperature for <15 seconds before washing with 600 μl ice-cold MQ H_2O and drying with Ar. Samples were cured for at least 20 min before scanning. Filaments were visualized on a NanoScope V controller with TESPA-V2 tips (Bruker). Images were analyzed for changes in topology and height with Gwyiddion software (available at http://gwyddion.net; Ref. 68). Filaments were categorized as linear, bridged or multi-bridged based on the number of DNA ends visible in each filament image.

DNA bridging pulldown assay

These experiments were performed as previously described (R. A. van der Valk, *et al.,* submitted for publication in Methods in Molecular Biology and Ref. 39) with some minor modifications. Streptavidin-coated paramagnetic Dynabeads M280 (Invitrogen) were washed once with 100 μl of 1× phosphate-buffered saline and twice with Coupling Buffer (CB: 20 mM Tris–HCl pH 8.0, 2 mM EDTA, 2 M NaCl, 2 mg acetylated BSA/ml, 0.04% Tween20) according to manufacturer instructions. After washing, the beads were resuspended in 200 μl CB containing 100 nM biotinylated DNA (bait). The DNA used was a 685 bp, random AT-rich (32% GC) sequence prepared as described in (39). Note the sequence used for this assay is not the same as that used for *in vitro* transcription or AFM experiments. Next, the bead suspensions were incubated for 30 minutes on a rotary shaker (1 000 rpm) at 25°C. After incubation, the beads were washed twice with Incubation Buffer (IB: 40 mM HEPES-KOH pH 8.0, 5% glycerol, 0.022% NP-40, 0.1 mg acetylated BSA/ml; IB may be supplied with various concentrations of magnesium aspartate or potassium glutamate depending on the experiment; see Figure 6) before resuspension in IB and addition of ∼8 000 cpm of radioactively end-labeled ^{32}P 685 bp DNA (2 μl of DNA; prey). Radioactive DNA was supplemented with unlabeled 685 bp DNA to maintain a constant (20 nM) DNA concentration. The DNA bridging proteins H-NS, StpA or an equimolar mixture of H-NS and StpA (concentrations indicated in the text and Figure 6) were added and the mixture was incubated for 20 min on a shaker (1 000 rpm) at 25°C. To remove unbridged prey DNA, the beads were washed with IB before resuspension in 12 μl stop buffer (10 mM Tris pH 8.0, 1 mM EDTA, 200 mM NaCl, 0.2% SDS). All samples were quantified by liquid scintillation counting over 5 min. All values recovered from the DNA bridging assay were corrected for

background signal (using the signal generated from a sample lacking protein). DNA recovery (% of input) was calculated as a fraction of the signal recovered in each condition over the signal from a reference sample containing 2 μl of prey DNA. All experiments contained a total of 75 mM of monovalent ions from the protein storage buffers (15 mM KCl from H-NS and 60 mM NaCl from StpA); the presence of additional monovalent ions is explicitly stated in the experiment.

RESULTS

Hha and StpA modified the ability of linear H-NS filaments to stimulate robust RNAP pausing

Bridged H-NS filaments at 66 DBD/kb stimulate transcriptional pausing, but linear H-NS filaments at 200 DBD/kb have little effect on elongating RNAP (32). Thus, we first investigated whether Hha or StpA could alter the effect of H-NS on transcription at 200 DBD/kb filaments. To mimic transcription from the *bgl* antisense promoter into *bgl* H-NS filaments (5), we used a DNA template that contains *bgl* DNA positioned downstream from a λP_R promoter and C-less cassette so that transcription occurred into the DRE (Figure 2A and Supplementary Table S2). Transcription was initiated from λP_R without CTP, resulting in a halted EC containing a radiolabeled 26-mer nascent RNA (A26 EC). The A26 ECs were then incubated with H-NS, StpA, Hha or mixtures of these proteins. This method of generating halted A26 ECs before filament formation decoupled initiation and EC formation from transcript elongation through the filaments and avoided H-NS inhibition of initiation. We used the A26 ECs to form filaments (Figure 2A) by incubating them for 20 minutes at 20°C with (i) H-NS at 66 DBD/kb (bridged H-NS filament); (ii) H-NS at 200 DBD/kb (linear H-NS filament); (iii) 200 monomer/kb of Hha and 200 DBD/kb of H-NS (Hha:H-NS filament; note that Hha does not substitute for H-NS in a filament but binds to H-NS); (iv) StpA and H-NS at 100 DBD/kb of each (StpA:H-NS filament; note that StpA substitutes for H-NS in a filament giving 200 DBD/kb total); (v) 200 DBD/kb each of H-NS and StpA (400 DBD/kb total); or (vi) StpA at 200 DBD/kb (StpA filaments). The filament-containing ECs were then incubated with all four NTPs (30 μM each) and assayed for elongation and pausing by denaturing polyacrylamide gel electrophoresis (PAGE) of the radiolabeled RNA products (Figure 2B; Supplementary Figures S2 and 3). Note that we subsequently refer to H-NS or StpA filaments as H-NS-only or StpA-only filaments when necessary for clarity.

The effect of each type of filament on elongation was determined by comparing both the mean length and the range of transcript lengths comprising 30% of the total signal (15% in both the longer and shorter directions from the mean (see 'Materials and Methods' section; Figures 2C-D and 3; Supplementary Figure S2) for successive time points. Consistent with prior results (32), we observed a decrease in the MTL relative to transcription of naked DNA in conditions that induce formation of bridged H-NS filaments, but not conditions that allow formation of linear H-NS filaments (Figures 2D and 3A; Supplementary Figure S2, compare red and purple dots). Both Hha- and StpA-containing filaments exhibited striking differences compared to linear H-NS-only filaments. MTLs in the presence of StpA:H-NS filaments were similar to those of bridged H-NS filaments rather than linear ones (Figures 2D and 3B; Supplementary Figure S2, compare red to yellow and orange). The StpA and Hha:H-NS filaments decreased transcript lengths even further (Figures 2D, 3A and C; Supplementary Figure S2, blue and green).

During elongation on naked DNA, RNAP pauses at specific sequences on the *bgl* template (32), delaying elongation to the end of the DNA template. The decrease in MTL in the presence of bridged H-NS filaments is due to either the appearance of new pause sites or the enhancement of pauses that are present during elongation on naked DNA. To compare pauses stimulated by mixed filaments to H-NS-only filaments, we converted the gel lanes (Figure 2B and C; Supplementary Figures S2, 3, 5, 7 and 9) to pseudo-densitometry profiles (Figure 2E–G). In these profiles, the bridged H-NS filaments stimulated pausing at sites previously defined as H-NS sensitive and backtrack-prone (e.g. C346, Figure 2F; Ref. 32). The linear H-NS filaments did not stimulate pausing (e.g. note the level of C346 RNA in Figure 2F; Ref. 32). The Hha:H-NS filaments robustly stimulated a pause site nine nucleotides downstream of the A26 halt site (G35) along with other pauses between G35 and ~64 nt. The G35 pause and other pauses were not stimulated by bridged H-NS-only filaments (Figure 2E; Supplementary Figures S2 and 4). Stimulation of pausing at these short transcript lengths (<100 nt) by Hha:H-NS filaments explained the dramatic shortening of RNA products to an average length of <100 nt (Figure 2D).

Pause stimulation by StpA:H-NS filaments showed similarities to that induced by bridged H-NS filaments. The StpA:H-NS filaments stimulated the H-NS sensitive pauses at C346 and U588, consistent with the similar MTLs caused by StpA:H-NS and bridged H-NS filaments (Figure 2F, yellow line). Despite the same total DBD/kb of the StpA:H-NS filaments as the linear H-NS filaments (200 DBD/kb), the StpA:H-NS filaments strongly affected elongation to a level comparable to the bridged H-NS filaments and in contrast to the lack of effect of linear H-NS filaments. To rule out the possibility that the 200 DBD/kb StpA:H-NS filaments stimulated pausing due to formation of a 100 DBD/kb H-NS-only filament, we also formed StpA:H-NS filaments at 400 DBD/kb (Figure 2F, orange line). At 400 DBD/kb, an H-NS-only filament, if formed, would be 200 DBD/kb and linear, conditions in which H-NS has little effect on pausing (Supplementary Figure S8). However, we observed constitutive pause enhancement in these conditions (e.g. compare levels of C346 pause in Figure 2F), likely reflecting bridging mediated by StpA:H-NS filaments. In contrast, StpA filaments formed at 200 StpA/kb (the StpA level present in the 400 DBD/kb StpA:H-NS filaments) stimulated pausing at locations much earlier on the *bgl* template than were observed by StpA:H-NS filaments (e.g. G35 and other locations marked with asterisks; Figure 2G). The locations of the pauses stimulated by StpA filaments (the majority of which had lengths of <500 nt) agreed with the shorter MTL observed for StpA filaments compared to StpA:H-NS filaments. This result revealed a

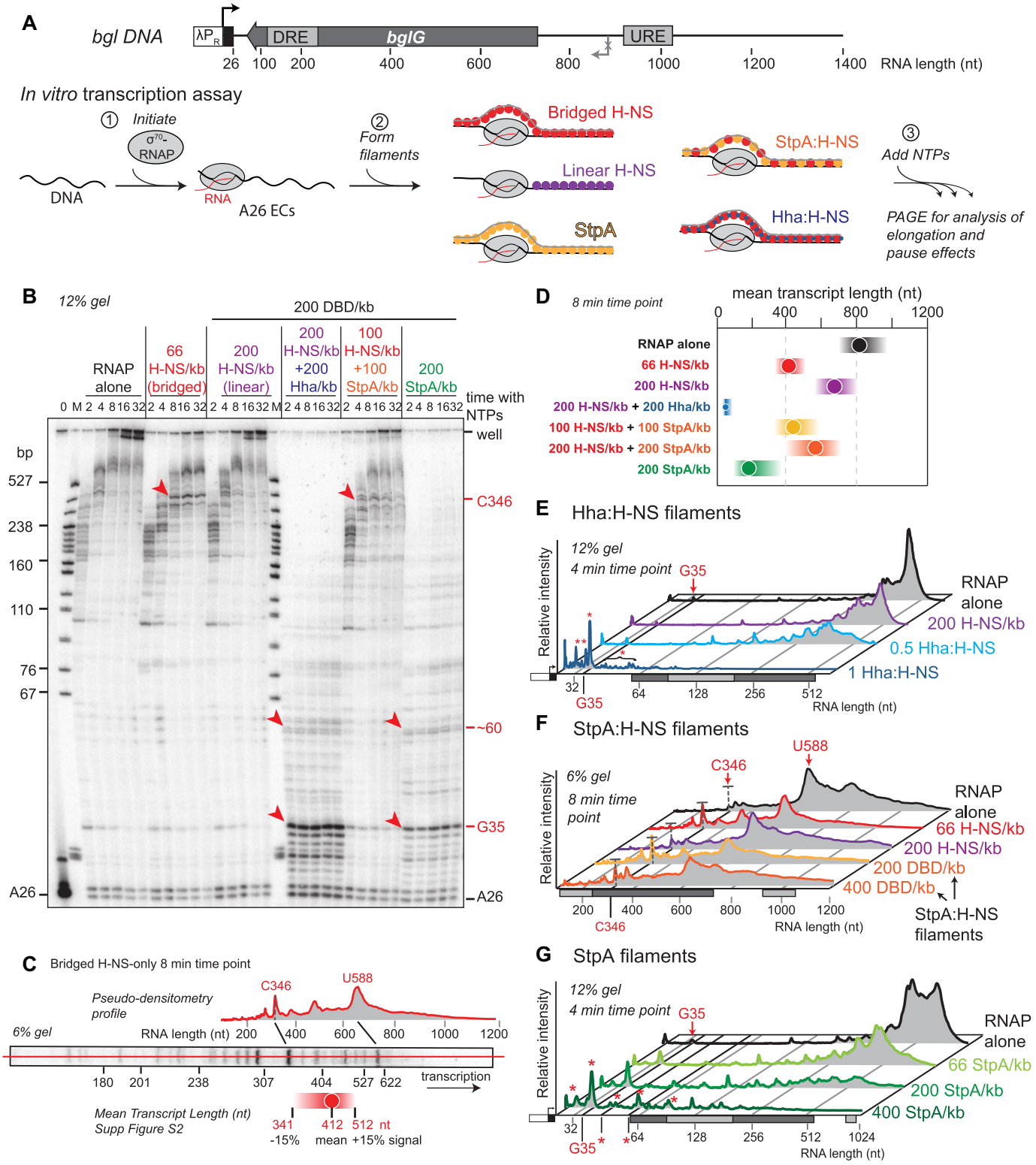

Figure 2. Hha and StpA modulate pause stimulation by H-NS-containing nucleoprotein filaments. (**A**) Experimental schematic and filament configurations. (Step 1) A26 ECs (10 nM) were formed by initiating RNAP-σ^{70} holoenzyme in the absence of CTP from the λP_R promoter on the 1.5 kb *bgl* template (top schematic and DNA; black or gray lines). To mimic the position of an antisense promoter and an H-NS filament in *bgl* operon, *bglG* is oppositely oriented to λP_R. The H-NS filament forms from two high-affinity H-NS binding sites (light gray; downstream regulatory element, DRE and upstream regulatory element, URE). Additionally, the canonical *bgl* promoter is found in this template (*gray antisense arrow with x*), but due to NTP withholding during initiation, formation of a filament across the promoter and the presence of a downstream intrinsic terminator (101), the promoter is likely inactive in our assay. (Step 2) Nucleoprotein filaments were formed on the EC-bound DNA using H-NS (red, bridged conformation; purple, linear conformation), Hha (blue) or StpA (yellow) alone or in the combinations shown. (Step 3) NTPs (30 μM) were added to enable RNAP elongation through the nucleoprotein

dramatic pause stimulation activity for StpA-only filaments that differed from the effect of StpA:H-NS filaments.

The results described above establish that linear H-NS filaments can become pause-stimulating filaments when either Hha or StpA are present during filament formation. The simplest hypothesis to explain these results is that Hha:H-NS and StpA:H-NS filaments are bridged, since bridged H-NS filaments are known to stimulate pausing. Because the H-NS/DNA ratio affects the ability of H-NS to stimulate pausing, we next tested the effect of varying the protein/DNA ratios for mixed filaments. Although StpA and H-NS are known to form 1:1 heterodimers *in vitro* (69), the stoichiometry of Hha to H-NS interaction is uncertain (17,21). Thus, we next tested the effects of different Hha:H-NS ratios.

At least 1:1 Hha:H-NS was required to slow RNAP elongation significantly

Hha is proposed to bind H-NS at either low (1 Hha per H-NS dimer, 0.5 Hha:H-NS) or equimolar (2 Hha per H-NS dimer, 1 Hha:H-NS) ratios in solution (17,21). We found that equimolar Hha, added to either bridged or linear H-NS filaments, caused robust stimulation of pausing (e.g. G35), whereas a lower ratio only slightly stimulated pausing (Figures 2E and 3A; Supplementary Figures S4–6). Based on the MTL, equimolar Hha:H-NS ratio at 200 H-NS/kb caused an overall reduction in the rate of elongation by a factor of ∼10 (Figure 3A). It also increased early pausing by RNAP so that ∼16% of ECs were at G35 and ∼40% of ECs were at positions between A26 and G35 (e.g. U30, C31, G34; Supplementary Figure S4B and C). When Hha was present at 0.5 Hha:H-NS on linear H-NS filaments, the MTL was reduced by a factor of ∼1.5 and the amount of G35 was not increased above levels seen with H-NS filaments (Figure 3A and Supplementary Figure S4). When 66 H-NS/kb was combined with equimolar amounts of Hha, ∼10% of ECs remain paused at G35 (Supplementary Figure S4) and overall elongation was reduced by a factor of ∼2.5 (Figure 3A and Supplementary Figure S5). These results suggest that, when equimolar with H-NS but not at lower ratios, Hha modifies both bridged and linear H-NS filaments in a way that stimulates robust pausing by RNAP.

StpA:H-NS filaments enhanced pausing at multiple protein/DNA ratios

Since the effects of H-NS filaments are dependent on the H-NS/DNA ratio, we next investigated whether the effects of StpA:H-NS filaments also were dependent on protein/DNA ratio. Equimolar StpA:H-NS filaments at 66, 200 and 400 DBD/kb enhanced late RNAP pausing at C346 and U588 compared to elongation on bare DNA (Figure 2F; Supplementary Figures S7 and 8). All StpA:H-NS filaments also reduced MTLs, which were more similar to those of bridged H-NS filaments than linear H-NS filaments (compare maroon, yellow and orange to red in Figure 3B, and purple in Figure 3A; Supplementary Figures S7 and 8). Additionally, StpA:H-NS filaments only slightly stimulated the G35 pause (∼4% of ECs pause; Supplementary Figure S8), which was affected by StpA and Hha:H-NS filaments, but not stimulated by H-NS filaments. These results revealed that StpA:H-NS filaments stimulated pausing over a range of DBD/DNA ratios in contrast to H-NS filaments, which do not stimulate pausing at high H-NS/DNA ratios (≥200 H-NS/kb; Figures 2F and 3B). The difference between StpA:H-NS filaments and H-NS filaments might result from specific DNA-binding or filament-forming properties of the StpA:H-NS heterodimer or of StpA homodimers, depending on which predominate in the mixed filaments.

StpA filaments increased RNAP pausing compared to StpA:H-NS filaments

To investigate the effects of StpA-only filaments further, we characterized the protein/DNA ratio-dependence of StpA filaments on RNAP progression. We formed StpA filaments on A26 ECs at concentrations ranging from 33 to 800 StpA/kb (Figures 2G and 3C; Supplementary Figure S9). As with StpA:H-NS filaments, slower overall elongation caused by pause stimulation occurred at all StpA/DNA ratios. Further, StpA filaments enhanced the G35 pause (∼10% of ECs pause; Supplementary Figure S4D) to a level comparable to the effect of Hha on the G35 pause (Figure 2E and Supplementary Figure S4), and reduced the MTL by a factor of ∼7 after 8 min (Figure 3C; compare 400–800 StpA/kb to RNAP alone). Although StpA and H-NS are paralogs, the effect of StpA filaments on elongating RNAP

filaments. Samples were removed after times indicated in (**B**) or other legends, processed and analyzed after denaturing PAGE to determine effects on elongation and pausing (see 'Materials and Methods' section). (**B**) PAGE (12% PA) resolving shorter RNA products from *in vitro* transcription. Time points are 2, 4, 8, 16 and 32 min after addition of 30 μM NTPs. Filaments were formed at 20°C with proteins indicated in the figure (See also Supplementary Figures S2, 3 and 7). Red arrows indicate pauses of interest. M indicates MspI digested pBR322 ladder. 0 indicates sample taken before addition of NTPs. (**C**) Example of a pseudo-densitometry profile generated by using ImageQuant to convert each 6 pixel-wide position on the gel image along the red line to an approximate RNA length by comparison to ssDNA markers separated on the same gel (see 'Materials and Methods' section). The relative RNA intensities were then plotted as a function of RNA length and MTLs were calculated from these distributions. (**D**) MTLs (circle) and distribution (15% in the longer direction and 15% in the shorter direction from the mean as indicated by the color gradient bars) calculated for transcription through filaments shown in (B) and (F) at 8 min after addition of 30 μM NTPs. MTLs shown are averages of at least three independent experiments (See also Supplementary Figure S2). (**E**) Pseudo-densitometry profiles after PAGE (12% PA) of RNA products present 4 min after addition of 30 μM NTPs to ECs on DNA alone or with 200 H-NS/kb and no Hha, 100 Hha/kb (0.5 Hha:H-NS) or 200 Hha/kb (1 Hha:H-NS) (see also Supplementary Figure S5). (**F**) Pseudo-densitometry profiles after PAGE (6% PA) of RNA products present 8 min after the addition of 30 μM NTPs to ECs on DNA alone or in the presence of 66 and 200 H-NS/kb or 1:1 StpA:H-NS filaments at 200 or 400 DBD/kb (see also Supplementary Figure S7). At C346, the capped gray dashed line in each condition is the same height for comparison of the pause peak height. (**G**) Pseudo-densitometry profiles after PAGE (12% PA) of RNA products present 4 min after the addition of 30 μM NTPs to ECs on DNA alone or in the presence of StpA filaments formed at 66, 200 or 400 StpA/kb (see also Supplementary Figure S9). For all profiles, features of the *bgl* DNA template as described in (A) are shown on the *X*-axis, and the positions of strong pauses are indicated by red asterisks. Note that the *X*-axis scale is different in (F) compared to (E) and (G). Each profile is representative of at least three independent experiments.

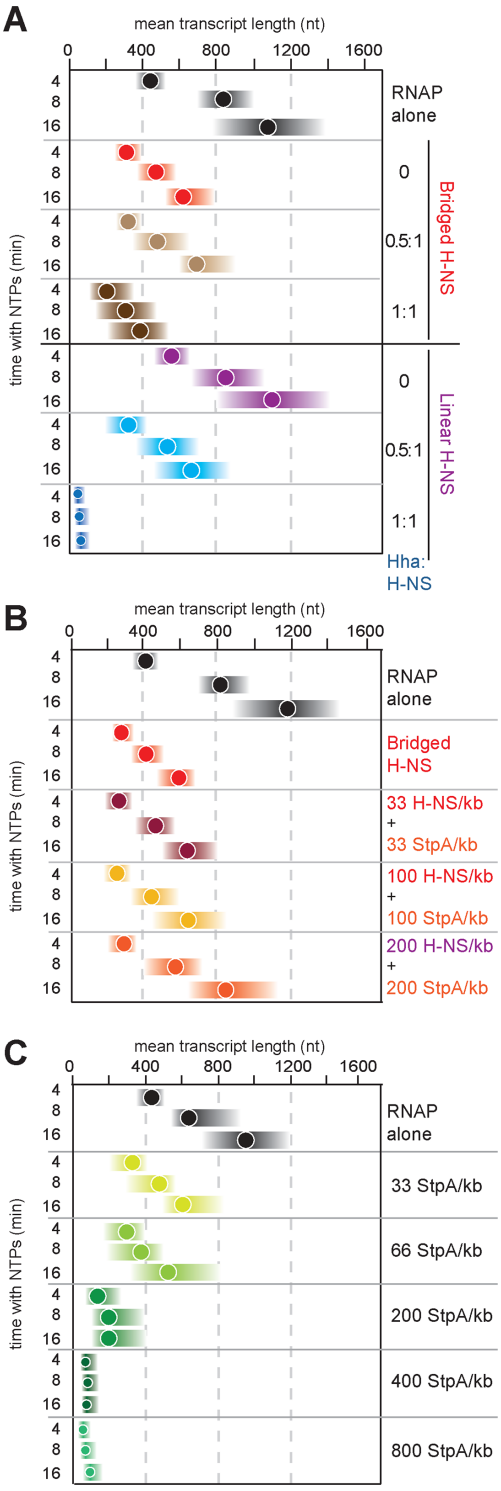

Figure 3. Hha:H-NS, StpA:H-NS and StpA filaments slow elongation over a range of protein concentrations. MTLs (circles) and length distributions (see legend to Figure 2) of RNA products present after 4, 8 and 16 min of transcription through nucleoprotein filaments at 30 μM NTPs. (**A**) Transcription through Hha:H-NS filaments formed with 0, 0.5:1 or 1:1 Hha:H-NS with 66 or 200 H-NS/kb (bridged and linear H-NS filaments, respectively). (**B**) Transcription through 1:1 StpA:H-NS filaments formed at 66, 200 and 400 total DBD/kb compared to bridged H-NS filaments (66 H-NS/kb). (**C**) Transcription through StpA filaments formed at 33, 66, 200, 400 and 800 StpA/kb. MTLs are averages of at least three independent experiments.

is more similar to that of Hha:H-NS filaments than that of H-NS filaments. Because StpA filaments strongly stimulate pauses at shorter transcript lengths (<100 nt) whereas the StpA:H-NS filaments mainly stimulate pauses in transcripts after synthesis of ∼300 nt, the StpA:H-NS filaments are likely composed of StpA:H-NS heterodimers (69). In other words, the StpA filaments are qualitatively different from H-NS or StpA:H-NS filaments, suggesting that patches of StpA-only filaments did not form when DNA was incubated with StpA:H-NS at a 1:1 ratio.

GreB effects suggest mixed filaments stimulate backtrack pausing by RNAP

We next sought to probe the nature of the pauses stimulated by mixed filaments. Bridged H-NS filaments preferentially stimulate backtracked pauses more than other classes of pauses (e.g. non-backtracked, elemental pauses; Refs. 32,70). Backtracking occurs when DNA and RNA reverse thread through RNAP, removing the 3′ end of the RNA from the active site and increasing the lifetime of pauses (Figure 4A; Refs. 32,71). Backtracked pauses stimulated by bridged H-NS filaments are suppressed by the addition of GreB (32), which promotes active-site cleavage of the displaced 3′ RNA (72), thereby allowing re-extension of the RNA from a non-backtracked register (Figure 4A). Given the similarities between effects of bridged H-NS filaments and Hha:H-NS and StpA:H-NS filaments, we hypothesized that mixed filaments might also enhance backtracked pauses but not elemental pauses.

To test this hypothesis, we assayed *in vitro* transcript elongation through mixed filaments in the presence of GreB (50 nM) at physiological NTP concentrations (1 mM each; enabling more rapid elongation). In the absence of GreB, pausing was still observed on the mixed filaments as found previously for H-NS filaments (Figure 4B and C, filled lines; Supplementary Figures S10 and 11; Ref. 32). Addition of GreB suppressed the G35, C346 and U588 pauses that were stimulated by StpA:H-NS and Hha:H-NS filaments. C346 and U588 are known pause sites susceptible to backtracking and pause stimulation by H-NS filaments (Figure 4B and C; Supplementary Figures S10 and 11). The effect of GreB on the G35 pause indicates that it is likely a backtrack pause (Figure 4C). Because mixed Hha:H-NS and StpA:H-NS filaments preferentially stimulate backtracked pauses similarly to the bridged H-NS filaments (32), the Hha:H-NS and StpA:H-NS filaments likely adopt a bridged conformation.

Hha:H-NS and StpA:H-NS filaments were preferentially bridged, whereas H-NS filaments switched between bridged and linear conformations

To examine potential bridging by Hha:H-NS and StpA:H-NS filaments directly, we next formed and visualized these filaments by EMSA and AFM (26,32). The *bgl* DNA and proteins were incubated together at 20°C for 20 min before either separating by native PAGE (EMSA) or applying to APS-treated mica for imaging by tapping-mode AFM (see 'Materials and Methods' section). As reported previously (32), H-NS filaments migrate at two distinct rates, with a

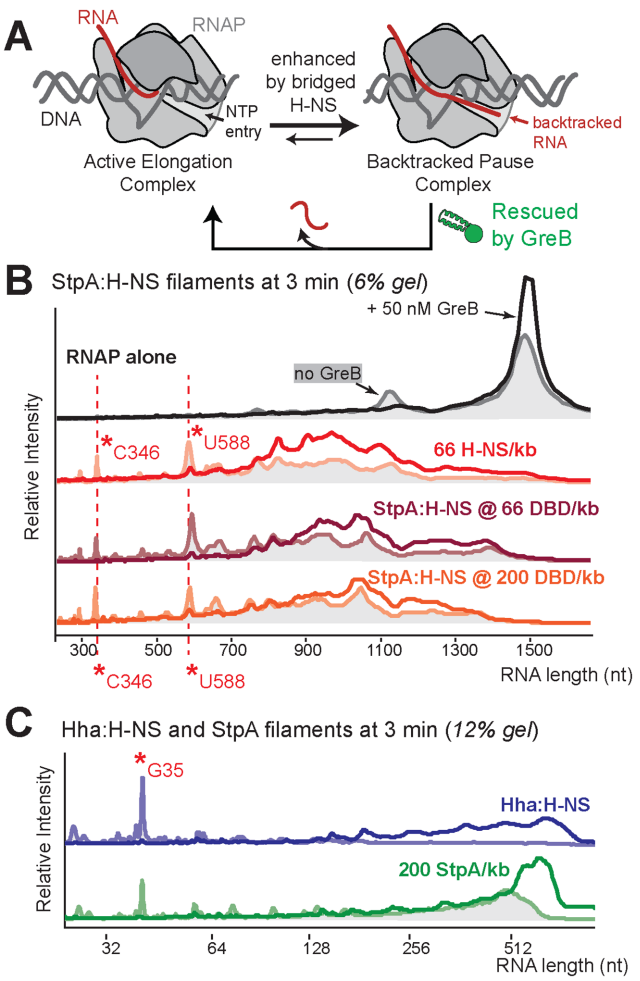

Figure 4. Mixed filaments stimulate backtracked pauses that can be rescued by GreB. (**A**) Active ECs (left) can add the next cognate NTP efficiently. At some pause sequences, the RNA (red) and DNA (dark gray) reverse thread through RNAP causing the 3′ end of the RNA to extrude out through the NTP-entry channel in RNAP in a backtracked pause state (right). GreB (green) can bind in the NTP-entry channel and stimulate cleavage by RNAP of the RNA to restore an active EC. Backtracked pauses are differentially enhanced by bridged H-NS filaments relative to non-backtracked pauses (32). (**B** and **C**) Pseudo-densitometry profiles after PAGE of RNA products present 3 min after addition of NTPs to 1 mM each in the absence (light, filled lines) or presence of (dark, non-filled lines) 50 nM GreB (B, 6% PA, see also Supplementary Figure S11; C, 12% PA, see also Supplementary Figure S10). Pauses stimulated by mixed filaments and reduced in intensity by GreB are indicated by red asterisks and dashed red lines. Nucleoprotein filaments in (B) were formed using 66 H-NS/kb (bridged filament conditions), StpA:H-NS at 66 DBD/kb or StpA:H-NS at 200 DBD/kb. Nucleoprotein filaments in (C) were formed using 200 Hha/kb plus 200 H-NS/kb or 200 StpA/kb. Data shown are from one of two independent experiments that gave similar results.

switch in electrophoretic behavior from slower to faster migration at the same H-NS/DNA ratio at which a switch from bridged to linear conformation is observed by AFM (slow migration and bridged filament at 66 H-NS/kb versus faster migration and linear filament at 200 H-NS/kb; Figure 5A, left and C; Supplementary Figure S12). In AFM, bridged and linear H-NS filaments can be distinguished by the number of double-stranded DNAs (dsDNAs) present in the filament. Typically, two dsDNAs are observed in bridged filaments (Figure 5C, panel iii), but one dsDNA is present in linear filaments (panel vi). Bridged H-NS filaments are unusual in two ways. First, they often form co-linear bridged filaments in which the same sequences in two DNA molecules align (confirmed by location of halted ECs near the co-linear ends of *bgl* DNA; see Figure 1 in Ref. 32). Second, they can also generate a circular conformation in which a single DNA forms a loop to provide the two DNA segments of the bridged filament (Figure 5C, panel iii; the circular conformation was not observed when RNAP was present Ref. 32). In our experiments, we observed ∼85% of the H-NS filaments in the bridged conformation at 66 H-NS/kb and ∼70% in the linear conformation at 200 H-NS/kb (Figure 5E and F), consistent with prior results (32).

Addition of Hha to H-NS filaments caused a dramatic change in filament conformation. The filaments appeared to be converted into a bridging mode, but with few co-linear bridged filaments observed. Instead, Hha:H-NS formed multi-bridged clusters that resembled the compacted filaments previously reported for StpA nucleoprotein filaments (26). In the EMSA, Hha:H-NS filaments that were formed at equimolar Hha:H-NS ratios (200 H-NS/kb) migrated as a broad smear that included species unable to enter the gel matrix (Figure 5A, right). The addition of more Hha (up to 3:1 Hha:H-NS) favored formation of the more slowly migrating species. The EMSA results suggested that Hha:H-NS formed a heterogeneous mixture of filaments with no discrete species (bands). To visualize Hha:H-NS filaments directly, we deposited Hha:H-NS filaments onto APS-mica and imaged the surface by AFM. A mixture of bridged filaments was apparent (Figure 5C, panel ii and Figure 5D), including both identifiable, discrete bridged filaments and large clusters of filaments (referred to as multi-bridged filaments). The complex network of DNAs in the clusters precluded precise quantitation of multi-bridged versus 1-1 bridged filaments (Figure 5D). The clusters were much larger in both height and width than bridged H-NS filaments, suggesting they contained many DNA molecules linked together by bridging H-NS and Hha molecules (Figure 5C, panel ii and Supplementary Figure S12D). Although AFM could not define the arrangement of Hha, H-NS and DNA within these clusters, the existence of these extreme DNA clusters was observed only in the presence of both Hha and H-NS (compare to Figure 5A, Hha-only lane). Notably, similar structures were observed at high H-NS/DNA ratios (28), indicating that Hha enables H-NS to adopt a similar structure even at less favorable ratios. These results suggest that Hha modifies H-NS/DNA nucleoprotein filaments and significantly promotes DNA bridging, thus enabling H-NS to bridge multiple DNA molecules.

StpA filaments were previously reported as primarily bridged (sometimes leading to compaction; Refs. 26,61,73). To understand the conformation of StpA filaments in our *in vivo*-like solute conditions (100 mM potassium glutamate and 8 mM magnesium aspartate; reviewed in Refs. 74,75), we examined these filaments using EMSA and AFM. Much like the Hha:H-NS filaments, StpA filaments appeared to prefer a bridged conformation and were prone to cluster multiple DNA molecules (Figure 5B, Figure 5C panels iv and vii; Figure 5E and F). At lower StpA/DNA ratios (66 StpA/kb), the EMSA revealed discrete StpA/DNA species

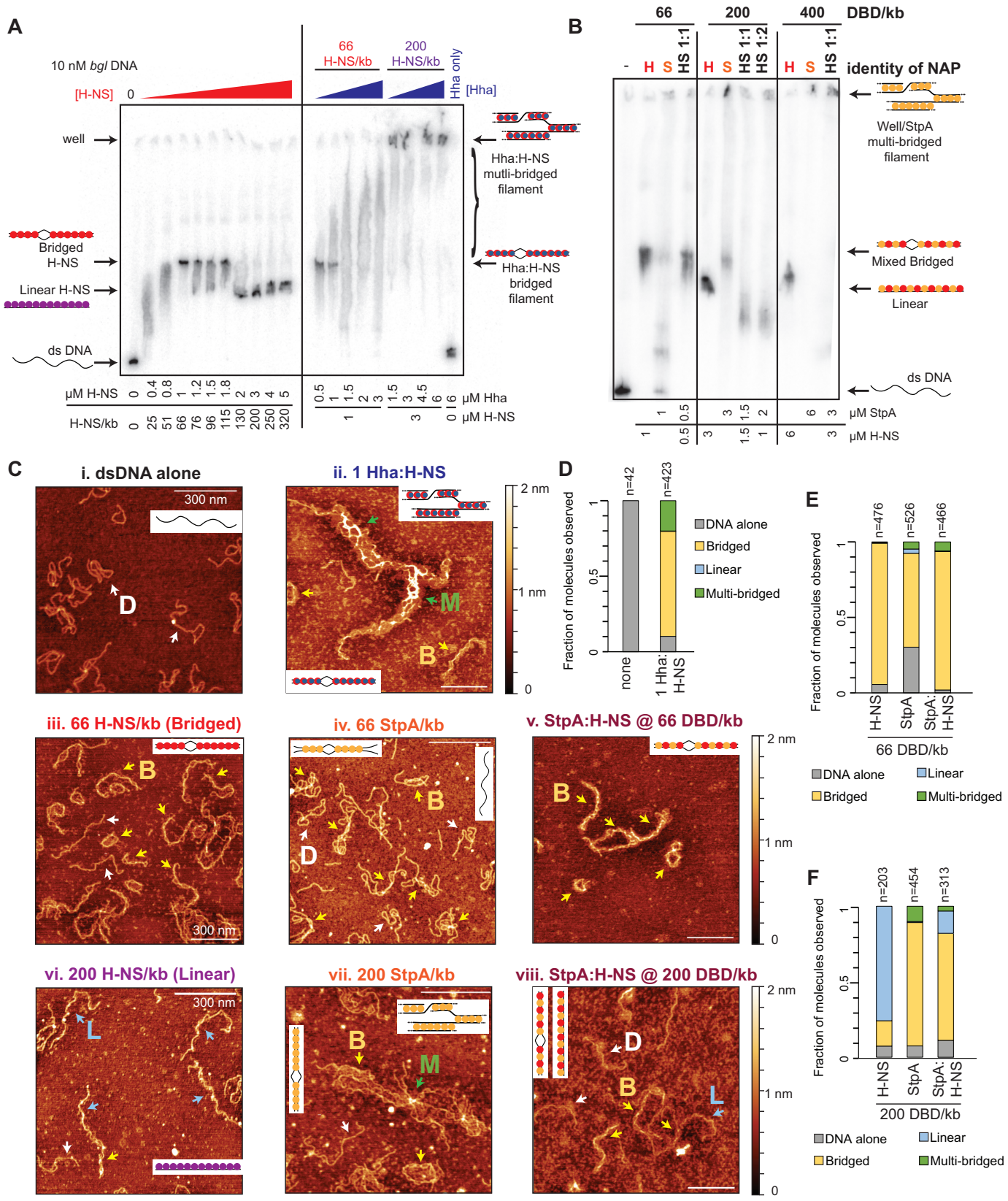

Figure 5. Hha:H-NS and StpA:H-NS form only bridged filaments, whereas H-NS forms both bridged and linear filaments. (**A**) Native PAGE (3% PA) of filaments formed by H-NS or Hha:H-NS on 10 nM 1.5 kb *bgl* DNA. H-NS ranged from 0 to 5 μM, for a range of 0 to 320 H-NS/kb as indicated (left panel). Hha was added at 0.5, 1, 1.5, 2 and 3 μM to 1 μM H-NS (66 H-NS/kb; bridged filaments) or at 1.5, 3, 4.5 and 6 μM to 3 μM H-NS (200 H-NS/kb; linear filaments) or at 6 μM Hha to DNA alone (right panel). Relevant species are indicated by arrows and pictograms (bridged H-NS, red;

that either migrated faster than bridged H-NS filaments or that migrated with the same mobility as bridged H-NS filaments (Figure 5B). In AFM, the 66 StpA/kb filaments were bridged (∼60% of objects had interconnected DNA segments; Figure 5E). The remaining molecules were either single dsDNA molecules lacking StpA (30%), multi-bridged clusters (∼%5) or linear filaments (∼5%) (Figure 5C, panel iv; Figure 5E). At 200 and 400 StpA/kb, the filaments migrated in native PAGE similarly to bridged H-NS filaments whereas others failed to migrate into the gel (Figure 5B). AFM confirmed that at 200 StpA/kb most (∼80%) filaments were bridged and some (∼10%) filaments appeared in a multi-bridged cluster resembling those observed for Hha:H-NS filaments (Figure 5C, panel vii; Figure 5F), possibly like compacted StpA/DNA filaments reported using different solute conditions (26). We conclude that StpA forms strikingly different nucleoprotein filament geometries than H-NS at the same protein/DNA ratios (compare 200 H-NS/kb and 200 StpA/kb; Figure 5F). These StpA filaments are mostly bridged, whereas H-NS filaments are mostly linear.

To examine the properties of StpA:H-NS filaments directly, we visualized the StpA:H-NS filaments at 66 and 200 DBD/kb by EMSA and AFM. In the EMSA, StpA:H-NS filaments at 66 DBD/kb migrated similarly to bridged H-NS filaments (Figure 5B); in AFM, nearly 75% of these StpA:H-NS filaments were bridged (Figure 5C compare panels iii to v; Figure 5E). However, under conditions that H-NS filaments are linear and not bridged, EMSA of StpA:H-NS filaments revealed both some filaments in the linear conformation and some filament aggregates that could not enter the gel (Figure 5B). AFM revealed that most filaments (∼70%) were bridged, but some were linear (∼15%) or multi-bridged clusters (∼5%; Figure 5C, panel viii, Figure 5F; Supplementary Figure S12). In the presence of 400 DBD/kb, the differences between StpA:H-NS filaments and H-NS filaments were more pronounced. In the EMSA, these StpA:H-NS filaments could not enter the gel whereas H-NS filaments gave a discrete (linear) band (Figure 5B). At all protein/DNA ratios tested, StpA:H-NS filaments favored bridged conformations (Figure 5E and F), consistent with the ability of StpA:H-NS filaments to stimulate pausing of RNAP at multiple protein/kb ratios (Figures 2 and 3).

As a more quantitative measure of bridging of the H-NS, StpA and StpA:H-NS filaments, we investigated their ability to bridge DNA by utilizing a DNA bridging pulldown assay (R.A. van der Valk, *et al.,* submitted for publication in Methods in Molecular Biology and Ref. 39). In this assay, the DNA bridging efficiency of a protein can be investigated over a wide variety of conditions. In this assay using a 685 bp AT-rich DNA that is different from our *bgl* DNA sequence, we observed that a higher critical protein concentration is required for DNA bridging by H-NS (6 μM) than by StpA (2 μM). Although we found that the critical protein concentration of the StpA:H-NS filament more closely resembled that of H-NS (5 μM instead of 4 μM), the percentage of DNA recovered by the mixed filament more closely resembled that of StpA (80%), than H-NS (50–60%). This observation indicates that the StpA:H-NS filament has properties resembling a combination of the individual proteins. Next, we investigated the dependence of these protein filaments on environmental cues. Again, in accordance with our abovementioned findings and the literature (26), we found that StpA outperformed H-NS in its ability to bridge DNA and was almost insensitive to Mg^{2+} concentration (Figure 6B) and K^{+} concentration (Figure 6C). Yet, when the proteins were combined, we observed mixed characteristics of the filament, displaying an almost equal distribution of the characteristics observed for H-NS or StpA filaments (Figure 6B and C). These solution experiments conclusively show that H-NS and StpA form a mixed filament and that the characteristics of both proteins are displayed evenly in the filament.

Overall, our analysis of filament conformations formed by Hha:H-NS and StpA:H-NS revealed that the mixed filaments are preferentially bridged independently of protein/DNA ratio and solute conditions, unlike H-NS-only filaments that switch from bridged to linear as H-NS/DNA ratios increase to levels that saturate DNA binding sites. These results are consistent with increased stimulation of pausing by Hha:H-NS and StpA:H-NS filaments based on the topological model of pause stimulation (described below).

←

linear H-NS, purple; Hha, blue). Two independent replicates of this experiment gave similar results. (**B**) Native PAGE (3% PA) of StpA:H-NS filaments formed at different total protein concentrations. H-NS and StpA were mixed at ratios of 1:1 or 1:2 for lanes labeled HS 1:1 or 1:2, respectively. StpA:H-NS filaments were compared to H-NS (H) and StpA (S) at the total protein concentrations indicated. Relevant species are indicated by pictograms. Three independent replicates of this experiment gave similar results. (**C**) Nucleoprotein filaments visualized by AFM (see 'Materials and Methods' section). Different protein combinations were incubated with *bgl* DNA before adsorption onto a mica surface. Representative images from at least two independent experiments of the following conditions are shown: (i) *bgl* dsDNA alone; (ii) 66 Hha/kb + 66 H-NS/kb (1 Hha:H-NS); (iii) bridged H-NS at 66 H-NS/kb; (iv) 66 StpA/kb; (v) StpA:H-NS filament with 33 StpA/kb + 33 H-NS/kb (66 DBD/kb); (vi) linear H-NS at 200 H-NS/kb; (vii) 200 StpA/kb; (viii) StpA:H-NS filament with 100 StpA/kb + 100 H-NS/kb (200 DBD/kb). Unbound DNA (D, white arrows), bridged filaments (B, yellow arrows), linear filaments (L, blue arrows) and multi-bridged filaments (M, green arrows) are indicated in each panel. Unbound DNA (dsDNA alone), linear filaments, bridged filaments and multi-bridged filaments were identified based on the number of visible DNA ends and on the height of the complexes above the mica surface. The *Z*-axis (height) color scale is shown on the right. Scale bars for each panel are 300 nm. Pictograms of the predominant filament types are shown in the insets. Larger scan areas for each image are shown in Supplementary Figure S12. (**D**–**F**) Classification and relative amounts of unbound DNA and bridged, linear and multi-bridged filaments for DNA alone and Hha:H-NS filaments (D), filaments at 66 DBD/kb (E) and filaments at 200 DBD/kb (F). Unbound DNAs, linear filaments (one DNA duplex per H-NS filament), bridged filaments (two DNA duplexes per H-NS filament) and multi-bridged filaments (more than two DNA duplexes per H-NS aggregate) each were counted as one complex ($n = 1$). The total number of complexes counted for each condition (n) is given above each bar (see Supplementary Figure S12). Although only ∼20% of observable objects were multi-bridged filaments for the Hha:H-NS filament condition (D), the fraction of DNA molecules in multi-bridged versus singly bridged filaments is much higher than the ratio of these complexes because each multi-bridged filament contains many DNAs. The number of DNAs in multi-bridged filaments was impossible to calculate due to compaction of DNAs in the complexes.

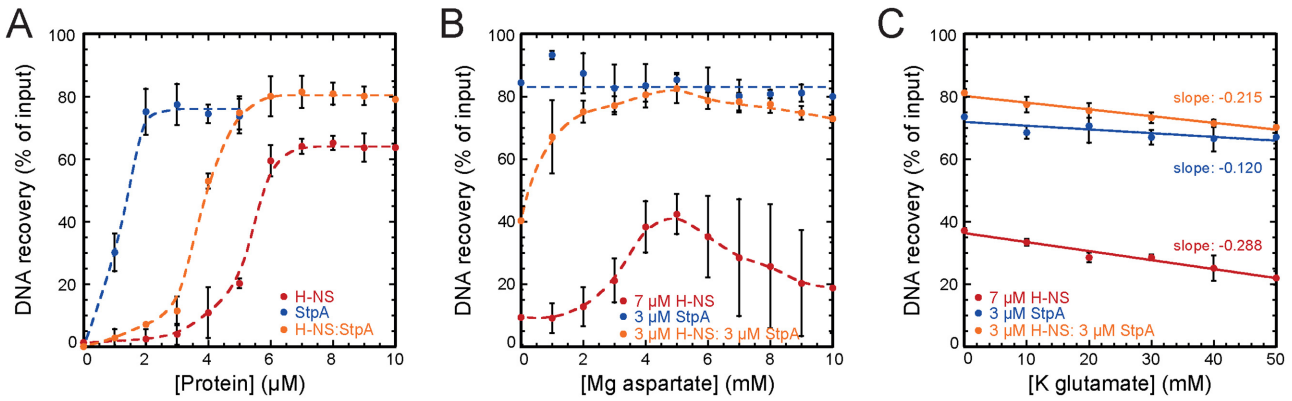

Figure 6. StpA filaments bridge DNA robustly compared to mixed filaments and weak H-NS filament bridging. (**A**) DNA recovery (as a percentage of the input DNA) as a function of H-NS (red), StpA (blue) or StpA:H-NS (orange) concentration as measured by the DNA bridging pulldown assay in the presence of 5 mM magnesium aspartate. (**B**) DNA recovery by H-NS (red), StpA (blue) or StpA:H-NS (orange) as a function of magnesium aspartate concentration. (**C**) DNA recovery by H-NS (red), StpA (blue) or StpA:H-NS (orange) as a function of potassium glutamate concentration in the presence of 5 mM magnesium aspartate. Solid lines were a fit by a linear regression model to calculate slopes, as indicated. Dotted lines (panels A and B) are to guide the eye. Data are plotted as mean values and the error bars represent the standard deviation from independent triplicate measurements.

Greater pause stimulation by mixed H-NS filaments was only partially explained by upstream bridged filament formation

A possible reason that Hha:H-NS and StpA filaments stimulate pausing much closer to the promoter than H-NS filaments is that the former but not the latter can trap early ECs in a topologically constrained domain by bridging with the short DNA available upstream from these early pause positions (Figures 2A and 7A). To test this possibility, we created the *upstream* template that contained 500 bp of DNA (from the H-NS-silenced *hlyC* gene) upstream of the λP_R promoter in the *bgl* template versus the 80 bp upstream in our standard *bgl* template (Figure 7B). The additional DNA sequences should ensure formation of bridged filaments upstream of halted A26 ECs or G35 paused ECs and could enhance H-NS stimulated pausing at G35 and other pauses at positions <300 nt if filament formation on both sides of an EC is sufficient to enhance pausing. However, we observed only a partial increase in pausing in the 40–300 nt range (Figure 7C, compare the amount of signal 15% below the MTL and no significant stimulation of the G35 pause by H-NS alone on the upstream template to effects of Hha:H-NS and StpA filaments presented in Figure 2). We calculated pause strength for three pause locations (G35, ∼80 nt, and ∼96 nt pauses; Figure 7C and D, gray dashed lines), which confirmed that the additional upstream DNA sequences had no significant effect on the G35 and 96 nt pauses. However, we did observe an ∼4-fold increase in pause strength at the 80 nt pause on the *upstream* template. These results suggest that the increased pause stimulation by Hha:H-NS or StpA filaments relative to H-NS filaments can only be partially explained by an improved ability to form bridged filaments on short upstream DNA. Therefore, an additional mechanism must explain why the Hha:H-NS and StpA filaments stimulate the G35 pause more robustly than H-NS filaments (see 'Discussion' section).

StpA:H-NS and StpA filaments stimulated robust pausing at 37°C and 20°C, but H-NS and Hha:H-NS filaments strongly stimulated pausing only at 20°C

Given the differences in effects on pausing among H-NS, StpA, StpA:H-NS and Hha:H-NS filaments, we wondered if the filaments would respond differently to environmental signals such as changes in temperature. We previously found that H-NS filaments do not stimulate pausing at 37°C, consistent with a proposal that H-NS silencing of pathogenic genes is relieved at higher temperatures (e.g. silencing at ∼22°C is lost at 37°C; Refs. 32,38). Changes in NAP composition are proposed to modulate the temperature-dependent regulation of many genes (76), including the type II secretion system genes (27), *ompW* (77,78) and the hemolysin operon (37,79). Since the *hly* operon, but not the *bgl* operon, is known to be regulated by temperature and by Hha, we used *hly* DNA to test the effect of temperature on transcription through mixed H-NS filaments. To test whether filament composition alters temperature effects of H-NS filaments, we formed filaments at either 20 or 37°C on a halted EC-containing *hly* DNA template that contained the Hha:H-NS-silenced 5′-leader region, *hlyC* and *hlyA* downstream from the halted EC (*hly* template, Figure 8A and Supplementary Figure S13A). Transcription through the filaments was assayed by addition of all four NTPs (1 mM each). Like the *bgl* template, the *hly* template allows decoupling of EC formation and subsequent NAP filament formation and transcript elongation.

At 20°C, Hha:H-NS, bridged H-NS, StpA and StpA:H-NS filaments, but not linear H-NS filaments, stimulated RNAP pausing on the *hly* template similarly to the observed pausing on the *bgl* template (Figure 8B; Supplementary Figures S14 and 15). Multiple pauses were stimulated, including some NAP-specific pauses at G35, ∼310, ∼450 and ∼625 nucleotides (Figure 8B, red lines). Pause stimulation by bridged H-NS or StpA:H-NS filaments reduced MTL by a factor of ∼1.5, whereas Hha:H-NS and StpA filaments reduced MTL by a factor of ∼3 (Figure 8B, magenta lines and Supplementary Figure S13). Interestingly, many

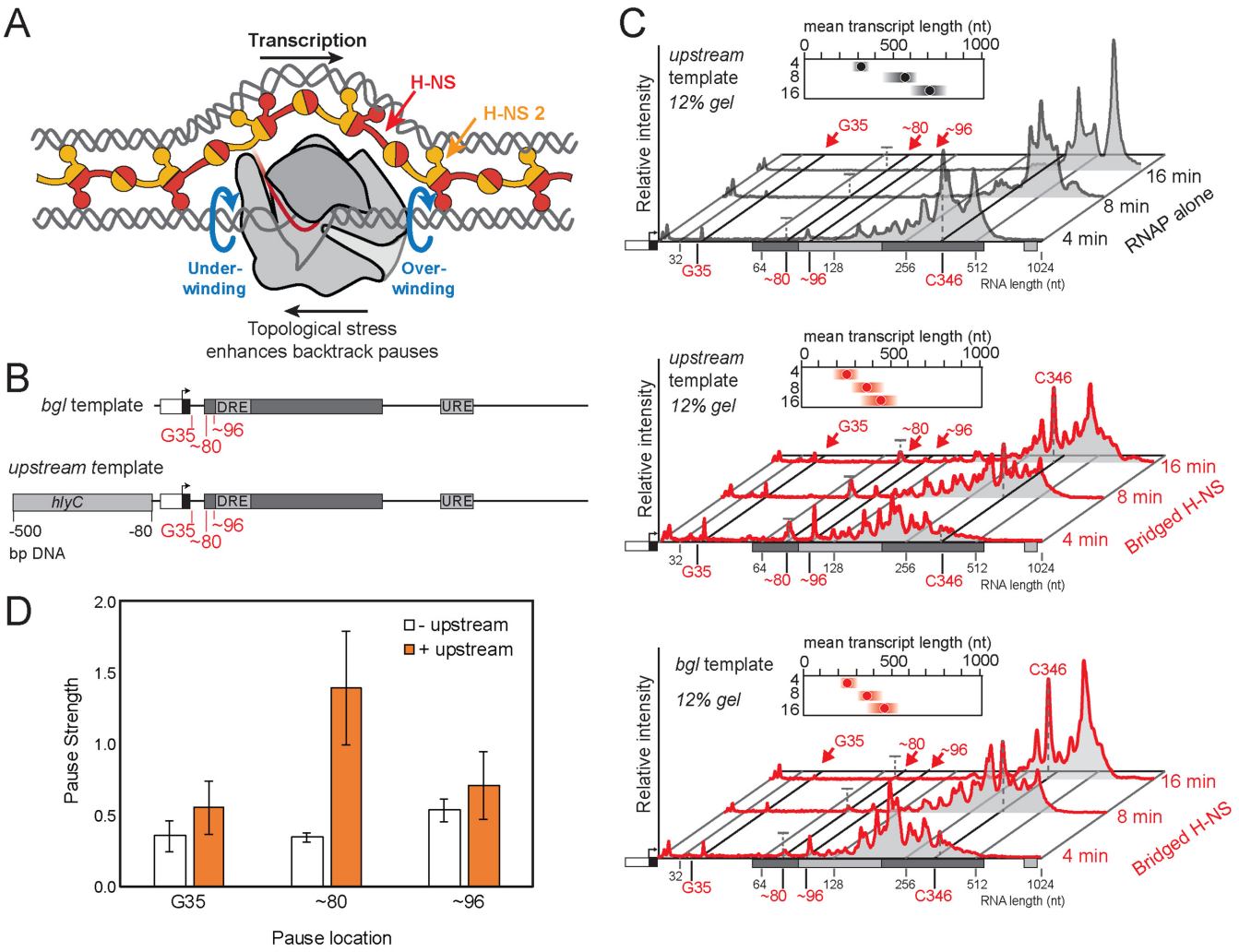

Figure 7. Stronger bridging around the EC partially explains the ability of mixed filaments to stimulate pausing. (**A**) Proposed model for stimulation of backtracked pauses during transcription of bridged H-NS filaments (32). Bridged filaments (red and yellow, alternating H-NS monomers) form around the EC (RNAP, gray; RNA, red; DNA, gray). Over-winding in front and under-winding of the DNA behind the EC (blue arrows) is generated by transcription when neither RNAP nor DNA can rotate freely; the resulting topological stress can be reduced by backtracking at pause sites. (**B**) Schematics of templates compared in this experiment. DNA sequence downstream of the promoter is the same for both templates. In the *upstream* template, 500 bp of *hlyC* DNA known to bind H-NS (light gray; see also Figure 8) was added upstream of the λP_R promoter. Pause sites of interest are marked (red). Other template features are indicated as described in the legend to Figure 2. (**C**) Pseudo-densitometry profiles of RNA transcripts formed on the *upstream* template 4, 8 or 16 min after the addition of 30 μM NTPs in the absence (top) or presence (middle) of bridged H-NS filaments (66 H-NS/kb) and profiles of transcripts formed on the *bgl* template with bridged H-NS filaments (bottom). Relevant pauses are indicated by red arrows. The capped gray dashed bar is the same height in each plot for comparison. Features of the DNA template are shown on the *X*-axis as in (B). MTLs and the distribution of RNA products from three independent experiments are shown above each profile. (**D**) Pause strengths for pausing at three locations (G35, ~80 nt and ~96 nt) on templates without (white) or with (orange) upstream DNA. Pause strengths were calculated as described previously (66).

pauses were located within the 5′ leader region, where they could potentially participate in regulation of the *hlyCABD* operon. This region contains the well-characterized backtracked pause site called *ops* (80), which functions in recruitment of the transcription factor RfaH; pausing at *ops* was enhanced by the bridged filaments. These results establish that mixed filaments slow elongation similarly on multiple templates that contain AT-rich DNA and are known to be silenced by H-NS (32).

At 37°C, StpA and StpA:H-NS filaments robustly stimulated pauses at G35, ~310, ~450 and ~625 nt and reduced the MTL by factors of ~4.5 and ~1.6 at 20 s, respectively, compared to RNAP alone (Figure 8C, yellow and green traces; Supplementary Figures S14 and 15). Importantly, the pause stimulation pattern of StpA:H-NS filaments was different than that of StpA filaments at both temperatures, suggesting that an StpA:H-NS filament, not an StpA-only filament that displaced H-NS, stimulated pausing at 37°C. In contrast, the H-NS and Hha:H-NS filaments gave only slight pause stimulation at 37°C compared to 20°C (Figure 8, compare red and blue traces in B and C). H-NS and Hha:H-NS filaments reduced MTL after 90 s at 20°C by a factor of ~1.5 and ~2.3, respectively, whereas neither filament reduced MTL by more than a factor of ~1.2 after 20 s at 37°C. The decreased effect of H-NS on transcript elongation at 37°C is consistent with our prior observation

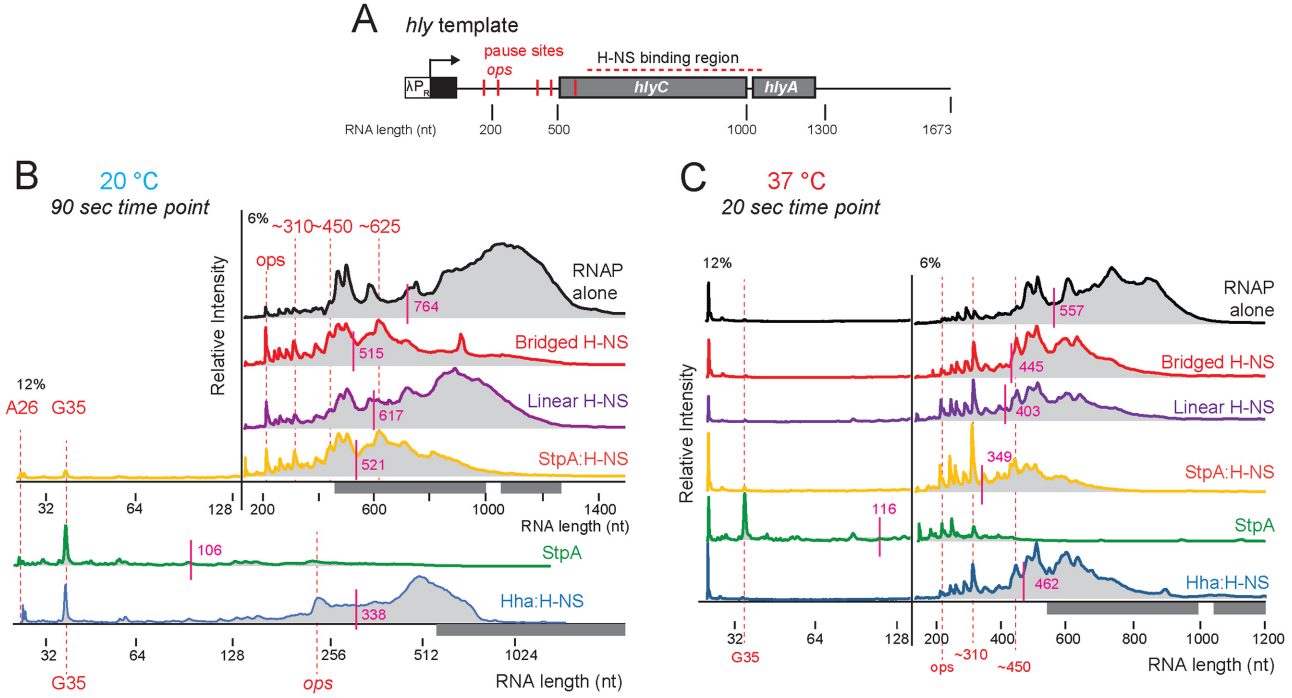

Figure 8. StpA:H-NS filaments stimulate pausing at 37°C more strongly than H-NS or Hha:H-NS filaments. (**A**) Schematic of *hly* template containing the 5′-UTR of the *E. coli* hemolysin operon followed by *hlyC* and a portion of *hlyA* (dark gray) downstream of the λP_R promoter and C-less cassette (black). RNAP initiates at the λP_R promoter and halts at A26 in the absence of CTP. NAP binding to the *hly* template was verified by EMSA (Supplementary Figure S13). Pause sites of interest are indicated (red). (**B**) Pseudo-densitometry profiles showing RNA products formed 90 s after elongation was restarted by addition of all 4 NTPs (1 mM each) at 20°C. After A26 EC formation, bridged and linear H-NS filaments were formed with 66 and 200 H-NS/kb, respectively. StpA:H-NS filaments were formed with equimolar StpA and H-NS at 66 DBD/kb. StpA filaments were formed with 200 StpA/kb. Hha:H-NS filaments were formed with 66 Hha/kb + 66 H-NS/kb. All reactions were incubated at 20°C for 20 min after protein addition and before NTP addition. (**C**) Pseudo-densitometry profiles of RNA transcripts formed 20 s after NTP addition at 37°C. Samples were from the same reaction mix as in (B) but were incubated at 37°C for 20 min before NTP addition. Gray bars on *X*-axis indicate the location of *hlyC* and *hlyA* genes in the *hly* template. Approximate location of pauses stimulated by filaments are indicated (red). MTLs (vertical magenta line on each profile) are averages from two independent experiments (Supplementary Figure S13). Profiles were generated by combining data from 12 to 6% PA gels (*left* and *right* of the solid black line, respectively); full gel images are shown in Supplementary Figures S14 and 15).

(32) and the relief of gene silencing at this temperature (38). The differential effects of StpA:H-NS and Hha:H-NS filaments on transcription at 20°C versus 37°C support a view that mixed filaments have specific properties that differ from those of H-NS filaments (see 'Discussion' section and Refs. 76,81).

DISCUSSION

The H-NS family of NAPs silences laterally transferred genes in enteric bacteria by forming mixed nucleoprotein filaments that repress both initiation and elongation of transcription. H-NS regulates some of these genes encoding diverse proteins responsible for pathogenesis and stress responses, which may explain the diversification of the H-NS family to include paralogs and modulators like StpA and Hha. We found that both Hha and StpA alter the ability of H-NS filaments to stimulate backtracked pauses so that stimulation occurs (i) more strongly; (ii) earlier in transcription units; (iii) with less dependence on protein/DNA ratio; and (iv), in the case of StpA:H-NS filaments, at higher temperatures. The ability of mixed filaments to stimulate pausing was correlated with increased propensity for bridging. Our *in vitro* results suggest potential mechanisms of H-NS-mediated pause stimulation and possible ways that Hha and StpA may fine-tune the response of H-NS filaments to environmental signals *in vivo*.

At least three mechanisms could contribute to bridged filament stimulation of pausing

Previously, we proposed a topological mechanism to explain the selective effect of bridged H-NS filaments on backtracking but not elemental pausing, and the lack of effect on pausing of non-bridged (linear) H-NS filaments (32). In the topological model of H-NS action, bridged filaments create a topologically closed domain by linking two DNAs together via bridging upstream and downstream of the EC (Figure 9A, *model 1*; Ref. 32). *In vitro* transcript elongation by an EC within this closed domain generates positive supercoiling downstream and negative supercoiling upstream unless the RNAP or DNA can rotate relative to each other as RNAP transcribes within the domain (the twin supercoiled domain model; Ref. 82). In the bridged filament, DNA rotation is restricted by bound H-NS, but could still occur as a function of the rate of transient release of DNA from H-NS contacts to diffuse the topological stress (Figure 9A, gray arrow in *model 1*). RNAP rotation will be restricted by steric clash and by potential entanglement of nascent RNA, both which will become more probable as the

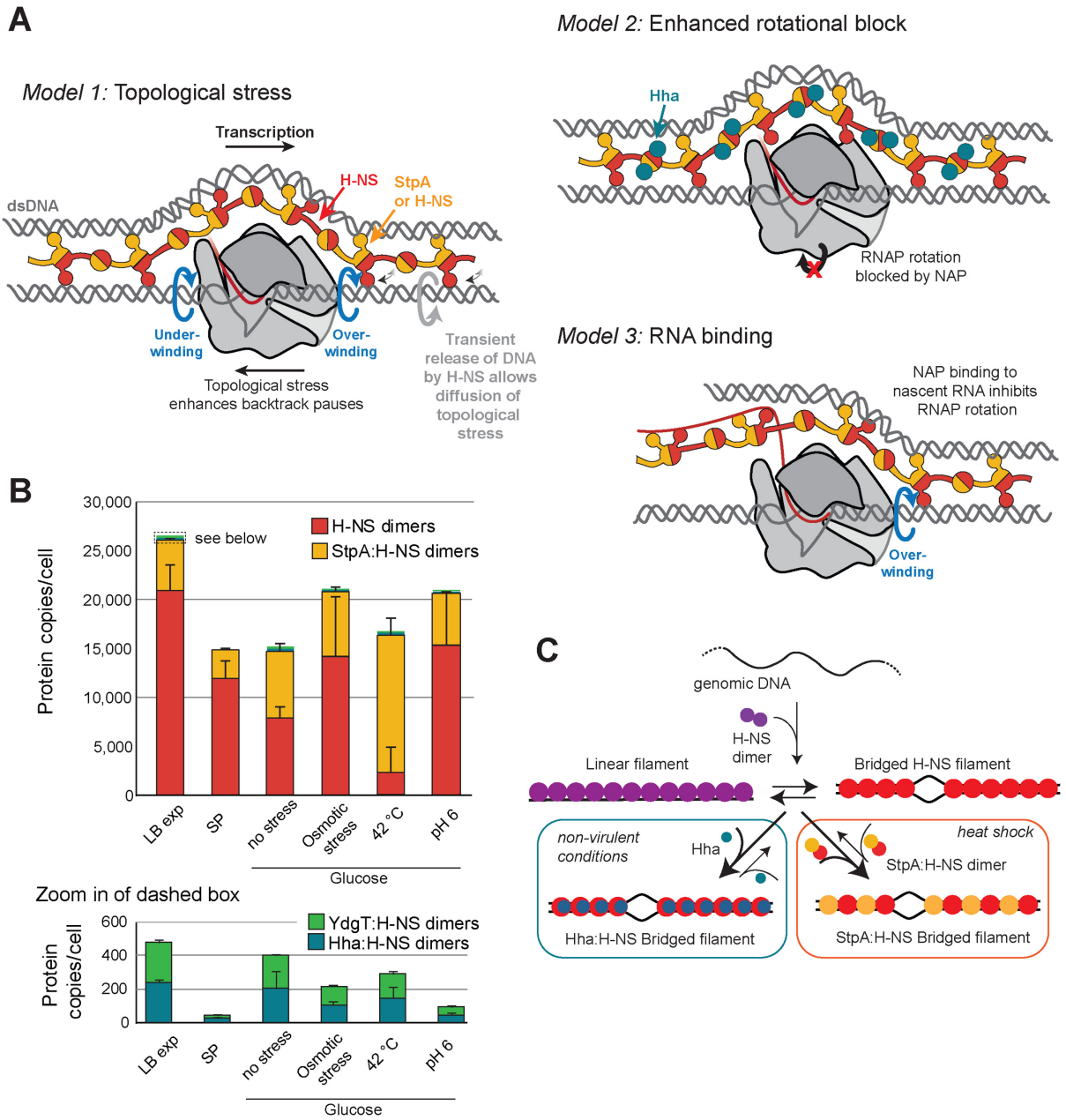

Figure 9. Models for stimulation of pausing by dynamic mixed filaments. (**A**) *Model 1*: Topological stress stimulates pausing. Bridged H-NS or StpA:H-NS filaments (alternating red and yellow monomers) with two DNA segments (gray) can form upstream and downstream of elongating RNAP (gray) and nascent RNA (red) (32). Hha (not shown for simplicity) could also be present in this filament. Upstream and downstream DNA binding domain contacts create a topologically closed domain that causes topological stress to accumulate because the RNA transcript blocks EC rotation sterically (positive supercoiling/over-winding downstream of RNAP and negative supercoiling/under-winding upstream of RNAP, blue arrows). This topological stress can be relieved by the backtracking of RNAP at pause sites. Additionally, dissociation of H-NS DBD (gradient double-sided arrow) could allow for diffusion of supercoiling to relieve topological stress (light gray arrow around *DNA*). *Model 2*: NAPs contribute to steric occlusion of RNAP rotation. Either StpA (yellow) or Hha (blue) in filaments may increase steric clash with rotating RNAP (black arrow) because they cannot rearrange all DNA binding surfaces to interact with a single DNA as appears to occur in linear H-NS filaments and could sequester displaced H-NS DBDs as shown in *model 1*. The greater steric clash may enhance topological stress described in *model 1*. Although we cannot exclude the possibility that that Hha and StpA create a direct steric block to RNAP translocation, this alternative would be predicted to enhance all pauses rather than selectively enhance backtrack pauses, as observed (see Figure 4). *Model 3*: NAPs bind nascent RNA. StpA, Hha (not shown for simplicity) or H-NS could bind to the nascent RNA directly and thereby inhibit RNAP rotation and enhance topological stress. (**B**) Levels of StpA:H-NS heterodimers (yellow), H-NS:H-NS dimers (red), Hha (blue) and YdgT (green) in *E. coli* K-12 grown in different conditions calculated from the monomer levels measured by quantitative mass spectrometry (45), assuming that all StpA present constitutively forms herterodimers with H-NS (69). Error bars from biological triplicates are shown for H-NS and StpA; the Hha and YdgT levels (dashed box) are shown in the bottom plot using a different scale. The growth conditions shown are exponential phase in LB (LB exp); stationary phase (SP); minimal media supplemented with glucose without stress, or with osmotic stress (50 mM NaCl), high-temperature stress (42°C) or acid stress (pH 6). (**C**) H-NS family filaments formed *in vivo* are likely in dynamic equilibrium between linear or bridged H-NS (purple and red, respectively), Hha (blue) bound filaments and StpA (yellow) bound filaments. This equilibrium could be influenced by different growth conditions (e.g. non-virulent growth or heat shock) and by sequences present in different genes.

length of RNA grows. Reverse threading of the nucleic acids in RNAP (i.e. RNAP backtracking) can relieve this topological stress (83). In this way, bridged H-NS filaments can stimulate backtrack pausing of RNAP and slow elongation even though H-NS dissociates too rapidly to explain pause stimulation via a direct steric block to forward translocation (k_{off} for bridged H-NS ~1.5 s^{-1}; Ref. 84). A linear filament would not create a topologically closed domain around RNAP. Thus, the topological model provides a simple explanation for the lack of effect of linear filaments on elongating RNAP *in vitro* and may contribute to increased pausing *in vivo*.

The topological model may also explain the greater stimulation by Hha and StpA of backtrack pausing by RNAP (Figure 9A, *model 1*), because Hha and StpA modulate H-NS filaments in ways that enhance bridging. However, the topological model alone does not explain why bridged H-NS filaments failed to stimulate pausing at positions <100 nt (e.g. G35), whereas Hha:H-NS and StpA:H-NS filaments strongly affect RNAP at these positions. Topological stress caused by DNA bridging should occur at any RNA length, provided neither the DNA nor EC can rotate. Even supplying additional DNA with affinity for H-NS upstream of +1 only slightly enabled H-NS filaments to stimulate pauses at ≤100 nt and did not replicate the robust effects of mixed filaments.

Three refinements of the topological model might explain the greater effects of mixed filaments on pausing *in vitro*: (i) StpA and Hha may increase the strength of DNA contacts and thus restrict diffusion of topological stress (stronger contacts in Figure 9A, *model 1*); (ii) StpA and Hha may increase steric inhibition of RNAP rotation around the DNA, which increases topological stress at shorter transcript lengths (Figure 9A, *model 2*); or (iii) StpA and Hha interactions with the nascent RNA transcript may inhibit RNAP rotation (Figure 9A, *model 3*).

Hha or StpA strengthens protein-DNA contacts in bridged nucleoprotein filament (Figure 9A, *model 1*). Such strengthened contacts may reduce diffusion of topological stress, effectively reducing the size of topological domains (85) and thereby increase backtrack pausing. It is possible that the site-specific effects of StpA (48) or Hha (17) could result from differences, relative to H-NS alone, in their sequence specificity of DNA binding. StpA or Hha may prefer to bind different sequences than H-NS, such as the +1 to +100 bp region of the *bgl* template. A difference in sequence preferences could impact which pauses are stimulated and might explain why Hha:H-NS or StpA filaments stimulate pauses between +1 and +100 more than H-NS-only. We also cannot exclude the possibility that tighter binding of StpA or Hha could create a direct steric clash that inhibits elongating RNAP; however, such direct inhibition of elongation does not readily explain why StpA and Hha, like H-NS, preferentially stimulate backtrack pausing.

Hha or StpA may increase the steric barrier to rotation of RNAP around the DNA (Figure 9A, *model 2*). Within the region of the bridged filament containing the EC, the H-NS or StpA DBD must be displaced from the DNA being transcribed. These displaced DBDs bound to the second DNA could create a steric block to rotation of RNAP, and this block could be greater when StpA or Hha is present. Thus, as RNAP elongates through the bridged filament, the filament may adopt a conformation that inhibits RNAP rotation to a greater or lesser extent. H-NS, which can form linear filaments, could relocate all its DBDs to the DNA molecule not being transcribed, so clash with RNAP is reduced. The displaced DBDs of StpA or associated Hha monomers, which cannot relocate to form linear filaments (39), might clash with the rotating RNAP to a greater extent (Figure 9A, *model 2*). Possibly, RNAP rotation *in vitro* could also become sterically more difficult as the transcript lengthens into a larger folded mass, which could synergize with inhibition of RNAP rotation by StpA or Hha.

A final and intriguing possibility is that the positively charged regions of H-NS, StpA or Hha might bind the nascent RNA directly (Figure 9A, *model 3*). In the context of the bridged topological domain model, such RNA interactions could either block RNAP translocation or rotation. Both H-NS and StpA have been shown to bind RNA (86,87); studies of RNA binding by Hha:H-NS have not been reported. Further mechanistic studies are needed to test if one or more of these models of nucleoprotein filament inhibition of transcript elongation described explain enhanced pause stimulation by StpA and Hha.

These three models are not mutually exclusive; aspects of them could operate together. Additionally, the relative contributions of these effects may differ *in vivo* from those we observed *in vitro*. For instance, RNAP rotation *in vivo* is more readily inhibited due to association of other molecules, notably ribosomes, with the nascent RNA and to RNAP (reviewed in Ref. 88). Supercoiling generated during transcription is relieved by topoisomerases *in vivo*, although it is unclear how readily topoisomerases access topological domains containing ECs within bridged filaments. Additionally, multiple RNAPs transcribing an operon *in vivo* might decrease the ability of filaments to slow elongation (89). Our *in vitro* results provide a biochemical framework for further study of bridged filaments effects, including *in vivo* studies.

StpA:H-NS filaments could increase gene silencing under stress conditions

The greater pause stimulation and temperature-resistance of the StpA:H-NS filament *in vitro* may be relevant to gene regulation *in vivo*. Assuming constitutive StpA:H-NS heterodimer formation (69), StpA:H-NS would make up ~30% of dimers in osmotic stress (the remainder would be H-NS homodimers) and would make up ~85% of the dimers at 42°C (compared to ~18% during exponential growth in LB; Figure 9B; Ref. 45). The distribution of these StpA:H-NS heterodimers throughout H-NS filaments during growth is unknown, although it is possible that StpA is localized to specific sequences (55). Our *in vitro* results suggest the propensity for DNA bridging will increase with greater StpA occupancy *in vivo* and these bridging interactions will persist at 37°C, whereas some H-NS occupied loci will lose transcriptional silencing at 37°C. Thus, the increases in StpA levels in stress conditions may function to elevate the extent of transcriptional silencing of some or all H-NS bound loci at higher temperatures (45). Additionally, the amount of StpA present within H-NS filaments may be

coordinated with other features, such as DNA conformational changes (90) to alter gene expression in response to changes in environment or temperature.

Some reported effects of StpA are consistent with this increased silencing model. In *Salmonella*, deleting *stpA* increases expression of some H-NS silenced genes, including *phoP* and other stress-response genes (91). In *E. coli*, deleting *stpA* in a Δ*hns* strain slows growth at 45°C (76) suggesting that StpA could contribute to silencing at elevated temperatures. Additionally, the constitutive bridging activity of StpA could make it relatively insensitive to changing environments and well suited for responding to stress. The preference of StpA for bridging might be due to sequence differences from H-NS in the 'buckle' region of the oligomerization domain. The H-NS buckle sequence is thought to allow flexibility between open and closed states in response to environmental factors (39). The StpA buckle may be locked in the open state, making StpA insensitive to changing conditions. Experiments investigating the consequences of *stpA* deletions or mutations in an *hns* background on stress survival are needed to understand the role of StpA in different environments.

Consistent with prior proposals (76), our results suggest that varying levels of StpA:H-NS heterodimers may target some H-NS-silenced genes under stress conditions, and that the consequence would be stabilized bridging, greater pause stimulation, and a high probability of Rho-dependent termination for these genes (Figure 9C). Additionally, the StpA:H-NS filament may be important for regulating initiation events, although it is unknown what role bridged filaments play in the occlusion of the promoter region. Further study is needed to understand potential differences in H-NS and StpA:H-NS DNA sequence binding specificities (Figure 9C) and how StpA modulates the characteristics of an H-NS filament.

Bridged Hha:H-NS filaments could aid in silencing virulence genes

The greater pause stimulation and bridging by Hha:H-NS filaments may be connected to the role of Hha in gene silencing *in vivo*. Hha is required to silence transcription of the hemolysin (*hly*) operon, which encodes components of a type 1 secretion system and hemolysin, HlyA (20,92 and reviewed in Ref. 93). The *hly* operon is induced by elevated temperature or high osmolality (20,37,94); *hly* is transcriptionally activated by RfaH, which recruits ribosomes that can subsequently suppress backtrack pausing and avoid premature Rho-dependent termination (32,35,80,95). Our results suggest Hha could be important for full repression of the *hly* operon, and other loci like it (e.g. the LEE operon (53) and acid-stress response genes, Ref. 63), by stimulating H-NS bridging and transcriptional pausing. Although Hha:H-NS filaments may repress transcription initiation (37,96), control of transcription elongation in *hly* must be paramount to explain transcriptional regulation by RfaH. The dramatically greater enhancement of pausing by Hha:H-NS likely explains full silencing of the hemolysin operon in non-infective conditions, although how RfaH regulates this activity is unknown. The temperature sensitivity of Hha-pause stimulation is consistent with the need to relieve the elongation block upon infection. The *hly* operon is likely regulated by a balance between Hha:H-NS filament stability and RfaH levels that increase termination and translationally coupled transcription, respectively, to coordinate expression to environmental conditions.

Our results suggesting 1:1 Hha:H-NS is the functional stoichiometry also raise important questions about the nature of Hha filaments *in vivo*. In *E. coli* K-12, levels of Hha are reported to be so low (Figure 9B; Ref. 45) that only one or two ∼2 kb Hha:H-NS filaments at 1:1 stoichiometry would exist. The levels of Hha do change in some conditions (Figure 9B); acid stress decreases Hha and osmotic stress increases Hha (49). However, Hha levels never approach those of H-NS. It is possible that Hha is more abundant in pathogenic strains; available data are all from non-pathogenic *E. coli* K-12 (Figure 9B; Ref. 45). If Hha is somehow localized to a subset of H-NS filaments, then an important outstanding question is the sequence dependence of this localization. The natural distribution of Hha *in vivo* is currently unknown; the only ChIP data were obtained with overexpressed Hha (63). Additionally, an Hha paralog, YdgT, is also present in *E. coli*, although also at low levels (Figure 9B; Ref. 45). YdgT can interact with H-NS and StpA (18,97), but may have effects similar to or different from Hha (39,63). Finally, our results provide more evidence that Hha enhances bridging of H-NS filaments (17,39) and possibly induces compaction (62); however, it remains unclear how Hha might drive H-NS to favor a multi-bridged conformation or how H-NS modulator proteins could reorganize H-NS filaments. An assessment of both *in vivo* Hha distribution and filament properties is essential to understand its effects on gene regulation.

Hha and StpA disrupt co-linearity of H-NS bridged filaments

An interesting and unanticipated finding of our current and earlier studies, unrelated to our goal of understanding effects on transcription, is that H-NS-only bridged filaments connect DNAs co-linearly such that the same sequences in two bridged molecules are aligned (Figure 5 and Ref. 32), but co-linearity is disrupted when Hha or StpA are present in bridged filaments. The physical basis of co-linear bridging and its disruption, whether it would occur in more complex mixtures of DNAs or *in vivo*, and whether it could play any role in sister locus cohesion during DNA replication (98) are unknown. The different behaviors of H-NS-only versus mixed bridged filaments (co-linear versus multi-bridged) suggest added complexity in nucleoid dynamics and gene silencing that merit further study.

CONCLUSION

Our results indicate that StpA and Hha stimulate H-NS bridging and pausing by RNAP, likely aiding gene silencing *in vivo*. Thus, the interplay between growth conditions and mixed filament formation suggests dynamic mechanisms of gene regulation in which nucleoprotein filaments of varying composition and silencing potentially form and disassemble in response to environmentally induced changes in H-NS paralog and modulator levels to adapt gene expression to growth conditions (Figure 9C). To define the roles

of mixed H-NS filaments in bacterial growth, survival and virulence, future studies should investigate how mixed filaments form, how H-NS paralogs may target different genes, and how bridged filaments stimulate RNAP pausing.

SUPPLEMENTARY DATA

Supplementary Data are available at NAR Online.

ACKNOWLEDGEMENTS

We thank Kalie Mix for help preparing APS for mica surface functionalization, Rod Welch for providing pSF4000, Ananya Ray-Soni and members of the Landick lab for helpful discussions, and Rachel Mooney and the anonymous referees for suggesting improvements to the manuscript.

FUNDING

NIH [GM38660 to R.L.]; Netherlands Organisation for Scientific Research (VICI) [016.160.613 to R.T.D.]; China Scholarship Council [201506880001 to L.Q.]; National Science Foundation Graduate Research Fellowship [DGE-1256259 to B.A.B.]; Department of Biochemistry, University of Wisconsin, Madison, William H. Peterson Fellowship (to B.A.B.). Funding for open access charge: NIH grant to R.L.
Conflict of interest statement. None declared.

REFERENCES

1. Barkay,T. and Smets,B.F. (2005) Horizontal gene flow in microbial communities. *ASM News*, **71**, 412–419.
2. Navarre,W.W., Porwollik,S., Wang,Y., McClelland,M., Rosen,H., Libby,S.J. and Fang,F.C. (2006) Selective silencing of foreign DNA with low GC content by the H-NS protein in *Salmonella*. *Science*, **313**, 236–238.
3. Lucchini,S., Rowley,G., Goldberg,M.D., Hurd,D., Harrison,M. and Hinton,J.C. (2006) H-NS mediates the silencing of laterally acquired genes in bacteria. *PLoS Path.*, **2**, e81.
4. Aznar,S., Paytubi,S. and Juárez,A. (2013) The Hha protein facilitates incorporation of horizontally acquired DNA in enteric bacteria. *Microbiology*, **159**, 545–554.
5. Peters,J.M., Mooney,R.A., Grass,J.A., Jessen,E.D., Tran,F. and Landick,R. (2012) Rho and NusG suppress pervasive antisense transcription in *Escherichia coli*. *Genes Dev.*, **26**, 2621–2633.
6. Ali,S.S., Xia,B., Liu,J. and Navarre,W.W. (2012) Silencing of foreign DNA in bacteria. *Curr. Opin. Microbiol.*, **15**, 175–181.
7. Stoebel,D.M., Free,A. and Dorman,C.J. (2008) Anti-silencing: overcoming H-NS-mediated repression of transcription in Gram-negative enteric bacteria. *Microbiology*, **154**, 2533–2545.
8. Ceschini,S., Lupidi,G., Coletta,M., Pon,C.L., Fioretti,E. and Angeletti,M. (2000) Multimeric self-assembly equilibria involving the histone-like protein H-NS. *J. Biol. Chem.*, **275**, 729–734.
9. Spurio,R., Falconi,M., Brandi,A., Pon,C.L. and Gualerzi,C.O. (1997) The oligomeric structure of nucleoid protein H-NS is necessary for recognition of intrinsically curved DNA and for DNA bending. *EMBO J.*, **16**, 1795–1805.
10. Tendeng,C. and Bertin,P.N. (2003) H-NS in Gram-negative bacteria: a family of multifaceted proteins. *Trends Microbiol.*, **11**, 511–518.
11. Madrid,C., Garcia,J., Pons,M. and Juarez,A. (2007) Molecular evolution of the H-NS protein: interaction with Hha-like proteins is restricted to enterobacteriaceae. *J. Bacteriol.*, **189**, 265–268.
12. Navarre,W.W. (2016) The impact of gene silencing on horizontal gene transfer and bacterial evolution. *Adv. Microb. Physiol.*, **69**, 157–186.
13. Zhang,A. and Belfort,M. (1992) Nucleotide sequence of a newly-identified *Escherichia coli* gene, *stpA*, encoding an H-NS-like protein. *Nucleic Acids Res.*, **20**, 6735.
14. Johansson,J., Eriksson,S., Sonden,B., Wai,S.N. and Uhlin,B.E. (2001) Heteromeric interactions among nucleoid-associated bacterial proteins: localization of StpA-stabilizing regions in H-NS of *Escherichia coli*. *J. Bacteriol.*, **183**, 2343–2347.
15. Johansson,J. and Uhlin,B.E. (1999) Differential protease-mediated turnover of H-NS and StpA revealed by a mutation altering protein stability and stationary-phase survival of *Escherichia coli*. *Proc. Natl. Acad. Sci. U.S.A.*, **96**, 10776–10781.
16. Madrid,C., Nieto,J.M. and Juárez,A. (2001) Role of the Hha/YmoA family of proteins in the thermoregulation of the expression of virulence factors. *Int. J. Med. Microbiol.*, **291**, 425–432.
17. Ali,S.S., Whitney,J.C., Stevenson,J., Robinson,H., Howell,P.L. and Navarre,W.W. (2013) Structural insights into the regulation of foreign genes in Salmonella by the Hha/H-NS complex. *J. Biol. Chem.*, **288**, 13356–13369.
18. Paytubi,S., Madrid,C., Forns,N., Nieto,J.M., Balsalobre,C., Uhlin,B.E. and Juárez,A. (2004) YdgT, the Hha paralogue in *Escherichia coli*, forms heteromeric complexes with H-NS and StpA. *Mol. Microbiol.*, **54**, 251–263.
19. Bae,S.H., Liu,D., Lim,H.M., Lee,Y. and Choi,B.S. (2008) Structure of the nucleoid-associated protein Cnu reveals common binding sites for H-NS in Cnu and Hha. *Biochemistry*, **47**, 1993–2001.
20. Nieto,J.M., Madrid,C., Prenafeta,A., Miquelay,E., Balsalobre,C., Carrascal,M. and Juárez,A. (2000) Expression of the hemolysin operon in *Escherichia coli* is modulated by a nucleoid-protein complex that includes the proteins Hha and H-NS. *Mol. Gen. Genet.*, **263**, 349–358.
21. Garcia,J., Madrid,C., Juárez,A. and Pons,M. (2006) New roles for key residues in helices H1 and H2 of the *Escherichia coli* H-NS N-terminal domain: H-NS dimer stabilization and Hha binding. *J. Mol. Biol.*, **359**, 679–689.
22. Solorzano,C., Srikumar,S., Canals,R., Juarez,A., Paytubi,S. and Madrid,C. (2015) Hha has a defined regulatory role that is not dependent upon H-NS or StpA. *Front. Microbiol.*, **6**, 773.
23. Paytubi,S., García,J. and Juárez,A. (2011) Bacterial Hha-like proteins facilitate incorporation of horizontally transferred DNA. *Cent. Eur. J. Biol.*, **6**, 879–886.
24. Rimsky,S., Zuber,F., Buckle,M. and Buc,H. (2001) A molecular mechanism for the repression of transcription by the H-NS protein. *Mol. Microbiol.*, **42**, 1311–1323.
25. Singh,S.S., Singh,N., Bonocora,R.P., Fitzgerald,D.M., Wade,J.T. and Grainger,D.C. (2014) Widespread suppression of intragenic transcription initiation by H-NS. *Genes Dev.*, **28**, 214–219.
26. Lim,C.J., Whang,Y.R., Kenney,L.J. and Yan,J. (2012) Gene silencing H-NS paralogue StpA forms a rigid protein filament along DNA that blocks DNA accessibility. *Nucleic Acids Res.*, **40**, 3316–3328.
27. Yang,J., Baldi,D.L., Tauschek,M., Strugnell,R.A. and Robins-Browne,R.M. (2007) Transcriptional regulation of the *yghJ-pppA-yghG-gspCDEFGHIJKLM* cluster, encoding the type II secretion pathway in enterotoxigenic *Escherichia coli*. *J. Bacteriol.*, **189**, 142–150.
28. Dame,R.T., Wyman,C. and Goosen,N. (2000) H-NS mediated compaction of DNA visualised by atomic force microscopy. *Nucleic Acids Res.*, **28**, 3504–3510.
29. Schroder,O. and Wagner,R. (2000) The bacterial DNA-binding protein H-NS represses ribosomal RNA transcription by trapping RNA polymerase in the initiation complex. *J. Mol. Biol.*, **298**, 737–748.
30. Dame,R.T., Wyman,C., Wurm,R., Wagner,R. and Goosen,N. (2002) Structural basis for H-NS-mediated trapping of RNA polymerase in the open initiation complex at the rrnB P1. *J. Biol. Chem.*, **277**, 2146–2150.
31. Shin,M., Song,M., Rhee,J.H., Hong,Y., Kim,Y.J., Seok,Y.J., Ha,K.S., Jung,S.H. and Choy,H.E. (2005) DNA looping-mediated repression by histone-like protein H-NS: specific requirement of E σ70 as a cofactor for looping. *Genes Dev.*, **19**, 2388–2398.
32. Kotlajich,M.V., Hron,D.R., Boudreau,B.A., Sun,Z., Lyubchenko,Y.L. and Landick,R. (2015) Bridged filaments of histone-like nucleoid structuring protein pause RNA polymerase and aid termination in bacteria. *eLife*, **4**, e04970.
33. Saxena,S. and Gowrishankar,J. (2011) Compromised factor-dependent transcription termination in a *nusA* mutant of *Escherichia coli*: spectrum of termination efficiencies generated by

perturbations of Rho, NusG, NusA, and H-NS family proteins. *J. Bacteriol.*, **193**, 3842–3850.
34. Saxena,S. and Gowrishankar,J. (2011) Modulation of Rho-dependent transcription termination in *Escherichia coli* by the H-NS family of proteins. *J. Bacteriol.*, **193**, 3832–3841.
35. Leeds,J.A. and Welch,R.A. (1997) Enhancing transcription through the *Escherichia coli* hemolysin operon, *hlyCABD*: RfaH and upstream JUMPStart DNA function together via postinitiation mechanism. *J. Bacteriol.*, **179**, 3519–3527.
36. Gaviria-Cantin,T., El Mouali,Y., Le Guyon,S., Romling,U. and Balsalobre,C. (2017) Gre factors-mediated control of *hilD* transcription is essential for the invasion of epithelial cells by *Salmonella enterica serovar Typhimurium*. *PLoS Path.*, **13**, e1006312.
37. Madrid,C., Nieto,J.M., Paytubi,S., Falconi,M., Gualerzi,C.O. and Juárez,A. (2002) Temperature- and H-NS-dependent regulation of a plasmid-encoded virulence operon expressing *Escherichia coli* hemolysin. *J. Bacteriol.*, **184**, 5058–5066.
38. Ono,S., Goldberg,M.D., Olsson,T., Esposito,D., Hinton,J.C. and Ladbury,J.E. (2005) H-NS is a part of a thermally controlled mechanism for bacterial gene regulation. *Biochem. J.*, **391**, 203–213.
39. van der Valk,R.A., Vreede,J., Qin,L., Moolenaar,G.F., Hofmann,A., Goosen,N. and Dame,R.T. (2017) Mechanism of environmentally driven conformational changes that modulate H-NS DNA-bridging activity. *eLife*, **6**, e27369.
40. Wolf,T., Janzen,W., Blum,C. and Schnetz,K. (2006) Differential dependence of StpA on H-NS in autoregulation of *stpA* and in regulation of *bgl*. *J. Bacteriol.*, **188**, 6728–6738.
41. Dole,S., Nagarajavel,V. and Schnetz,K. (2004) The histone-like nucleoid structuring protein H-NS represses the *Escherichia coli bgl* operon downstream of the promoter. *Mol. Microbiol.*, **52**, 589–600.
42. Nagarajavel,V., Madhusudan,S., Dole,S., Rahmouni,A.R. and Schnetz,K. (2007) Repression by binding of H-NS within the transcription unit. *J. Biol. Chem.*, **282**, 23622–23630.
43. Artsimovitch,I. and Landick,R. (2002) The transcriptional regulator RfaH stimulates RNA chain synthesis after recruitment to elongation complexes by the exposed nontemplate DNA strand. *Cell*, **109**, 193–203.
44. Bailey,M.J.A., Hughes,C. and Koronakis,V. (2000) *In vitro* recruitment of the RfaH regulatory protein into a specialised transcription complex, directed by the nucleic acid *ops* element. *Mol. Gen. Genet.*, **262**, 1052–1059.
45. Schmidt,A., Kochanowski,K., Vedelaar,S., Ahrne,E., Volkmer,B., Callipo,L., Knoops,K., Bauer,M., Aebersold,R. and Heinemann,M. (2016) The quantitative and condition-dependent *Escherichia coli* proteome. *Nat. Biotechnol.*, **34**, 104–110.
46. Talukder,A.A. and Ishihama,A. (2015) Growth phase dependent changes in the structure and protein composition of nucleoid in *Escherichia coli*. *Sci. China Life Sci.*, **58**, 902–911.
47. Talukder,A.A., Iwaki,T., Nishimura,A., Ueda,S. and Ishihama,A. (1999) Growth phase-dependent variation in protein composition of the *Escherichia coli* nucleoid. *J. Bacteriol.*, **181**, 6361–6370.
48. Sonnenfield,J.M., Burns,C.M., Higgins,C.F. and Hinton,J.C. (2001) The nucleoid-associated protein StpA binds curved DNA, has a greater DNA binding affinity than H-NS and is present in significant levels in *hns* mutants. *Biochimie*, **83**, 243–249.
49. Mourino,M., Balsalobre,C., Madrid,C., Nieto,J.M., Prenafeta,A., Munoa,F.J. and Juárez,A. (1998) Osmolarity modulates the expression of the Hha protein from *Escherichia coli*. *FEMS Microbiol. Lett.*, **160**, 225–229.
50. Sonden,B. and Uhlin,B.E. (1996) Coordinated and differential expression of histone-like proteins in *Escherichia coli*: regulation and function of the H-NS analog StpA. *EMBO J.*, **15**, 4970–4980.
51. Grainger,D.C., Hurd,D., Goldberg,M.D. and Busby,S.J. (2006) Association of nucleoid proteins with coding and non-coding segments of the *Escherichia coli* genome. *Nucleic Acids Res.*, **34**, 4642–4652.
52. Kahramanoglou,C., Seshasayee,A.S., Prieto,A.I., Ibberson,D., Schmidt,S., Zimmermann,J., Benes,V., Fraser,G.M. and Luscombe,N.M. (2011) Direct and indirect effects of H-NS and Fis on global gene expression control in *Escherichia coli*. *Nucleic Acids Res.*, **39**, 2073–2091.
53. Fukui,N., Oshima,T., Ueda,T., Ogasawara,N. and Tobe,T. (2016) Gene activation through the modulation of nucleoid structures by a horizontally transferred regulator, Pch, in enterohemorrhagic *Escherichia coli*. *PLoS One*, **11**, e0149718.
54. Uyar,E., Kurokawa,K., Yoshimura,M., Ishikawa,S., Ogasawara,N. and Oshima,T. (2009) Differential binding profiles of StpA in wild-type and h-ns mutant cells: a comparative analysis of cooperative partners by chromatin immunoprecipitation-microarray analysis. *J. Bacteriol.*, **191**, 2388–2391.
55. Srinivasan,R., Chandraprakash,D., Krishnamurthi,R., Singh,P., Scolari,V.F., Krishna,S. and Seshasayee,A.S. (2013) Genomic analysis reveals epistatic silencing of "expensive" genes in *Escherichia coli* K-12. *Mol. Biosyst.*, **9**, 2021–2033.
56. Lang,B., Blot,N., Bouffartigues,E., Buckle,M., Geertz,M., Gualerzi,C.O., Mavathur,R., Muskhelishvili,G., Pon,C.L., Rimsky,S. *et al.* (2007) High-affinity DNA binding sites for H-NS provide a molecular basis for selective silencing within proteobacterial genomes. *Nucleic Acids Res.*, **35**, 6330–6337.
57. Arold,S.T., Leonard,P.G., Parkinson,G.N. and Ladbury,J.E. (2010) H-NS forms a superhelical protein scaffold for DNA condensation. *Proc. Natl. Acad. Sci. U.S.A.*, **107**, 15728–15732.
58. Gao,Y., Foo,Y.H., Winardhi,R.S., Tang,Q., Yan,J. and Kenney,L.J. (2017) Charged residues in the H-NS linker drive DNA binding and gene silencing in single cells. *Proc. Natl. Acad. Sci. U.S.A.*, **114**, 12560–12565.
59. Liu,Y., Chen,H., Kenney,L.J. and Yan,J. (2010) A divalent switch drives H-NS/DNA-binding conformations between stiffening and bridging modes. *Genes Dev.*, **24**, 339–344.
60. Amit,R., Oppenheim,A.B. and Stavans,J. (2003) Increased bending rigidity of single DNA molecules by H-NS, a temperature and osmolarity sensor. *Biophys. J.*, **84**, 2467–2473.
61. Dame,R.T., Luijsterburg,M.S., Krin,E., Bertin,P.N., Wagner,R. and Wuite,G.J. (2005) DNA bridging: a property shared among H-NS-like proteins. *J. Bacteriol.*, **187**, 1845–1848.
62. Wang,H., Yehoshua,S., Ali,S.S., Navarre,W.W. and Milstein,J.N. (2014) A biomechanical mechanism for initiating DNA packaging. *Nucleic Acids Res.*, **42**, 11921–11927.
63. Ueda,T., Takahashi,H., Uyar,E., Ishikawa,S., Ogasawara,N. and Oshima,T. (2013) Functions of the Hha and YdgT proteins in transcriptional silencing by the nucleoid proteins, H-NS and StpA, in *Escherichia coli*. *DNA Res.*, **20**, 263–271.
64. Gibson,D.G., Benders,G.A., Andrews-Pfannkoch,C., Denisova,E.A., Baden-Tillson,H., Zaveri,J., Stockwell,T.B., Brownley,A., Thomas,D.W., Algire,M.A. *et al.* (2008) Complete Chemical Synthesis, Assembly, and Cloning of a *Mycoplasma genitalium* Genome. *Science*, **319**, 1215–1220.
65. Welch,R.A. and Pellett,S. (1988) Transcriptional organization of the *Escherichia coli* hemolysin genes. *J. Bacteriol.*, **170**, 1622–1630.
66. Theissen,G., Pardon,B. and Wagner,R. (1990) A quantitative assessment for transcriptional pausing of DNA-dependent RNA polymerase *in vitro*. *Anal. Biochem.*, **189**, 254–261.
67. Shlyakhtenko,L.S., Gall,A.A. and Lyubchenko,Y.L. (2013) Mica functionalization for imaging of DNA and protein-DNA complexes with atomic force microscopy. *Methods Mol. Biol.*, **931**, 295–312.
68. Nečas,D. and Klapetek,P. (2012) Gwyddion: an open-source software for SPM data analysis. *Open Phys.*, **10**, 181–188.
69. Leonard,P.G., Ono,S., Gor,J., Perkins,S.J. and Ladbury,J.E. (2009) Investigation of the self-association and hetero-association interactions of H-NS and StpA from enterobacteria. *Mol. Microbiol.*, **73**, 165–179.
70. Larson,M.H., Mooney,R.A., Peters,J.M., Windgassen,T., Nayak,D., Gross,C.A., Block,S.M., Greenleaf,W.J., Landick,R. and Weissman,J.S. (2014) A pause sequence enriched at translation start sites drives transcription dynamics *in vivo*. *Science*, **344**, 1042–1047.
71. Borukhov,S., Sagitov,V. and Goldfarb,A. (1993) Transcript cleavage factors from *E. coli*. *Cell*, **72**, 459–466.
72. Sosunova,E., Sosunov,V., Kozlov,M., Nikiforov,V., Goldfarb,A. and Mustaev,A. (2003) Donation of catalytic residues to RNA polymerase active center by transcription factor Gre. *Proc. Natl. Acad. Sci. U.S.A.*, **100**, 15469–15474.
73. Ali,S.S., Soo,J., Rao,C., Leung,A.S., Ngai,D.H.-M., Ensminger,A.W. and Navarre,W.W. (2014) Silencing by H-NS potentiated the evolution of Salmonella. *PLoS Path.*, **10**, e1004500.
74. Record,M.T., Courtenay,E.S., Cayley,D.S. and Guttman,H.J. (1998) Responses of *E. coli* to osmotic stress: large changes in amounts of cytoplasmic solutes and water. *Trends Biochem. Sci.*, **23**, 143–148.

75. Record,M.T., Courtenay,E.S., Cayley,D.S. and Guttman,H.J. (1998) Biophysical compensation mechanisms buffering *E. coli* protein-nucleic acid interactions against changing environments. *Trends Biochem. Sci.*, **23**, 190–194.
76. Müller,C.M., Schneider,G., Dobrindt,U., Emody,L., Hacker,J. and Uhlin,B.E. (2010) Differential effects and interactions of endogenous and horizontally acquired H-NS-like proteins in pathogenic *Escherichia coli*. *Mol. Microbiol.*, **75**, 280–293.
77. Xiao,M., Lai,Y., Sun,J., Chen,G. and Yan,A. (2016) Transcriptional regulation of the outer membrane porin gene *ompW* reveals its physiological role during the transition from the aerobic to the anaerobic lifestyle of *Escherichia coli*. *Front. Microbiol.*, **7**, 799.
78. Brambilla,L., Moran-Barrio,J. and Viale,A.M. (2014) Expression of the *Escherichia coli ompW* colicin S4 receptor gene is regulated by temperature and modulated by the H-NS and StpA nucleoid-associated proteins. *FEMS Microbiol. Lett.*, **352**, 238–244.
79. Duong,N., Osborne,S., Bustamante,V.H., Tomljenovic,A.M., Puente,J.L. and Coombes,B.K. (2007) Thermosensing coordinates a cis-regulatory module for transcriptional activation of the intracellular virulence system in *Salmonella enterica serovar Typhimurium*. *J. Biol. Chem.*, **282**, 34077–34084.
80. Artsimovitch,I. and Landick,R. (2000) Pausing by bacterial RNA polymerase is mediated by mechanistically distinct classes of signals. *Proc. Natl. Acad. Sci. U.S.A.*, **97**, 7090–7095.
81. Dorman,C.J. (2010) Horizontally acquired homologues of the nucleoid-associated protein H-NS: implications for gene regulation. *Mol. Microbiol.*, **75**, 264–267.
82. Liu,L.F. and Wang,J.C. (1987) Supercoiling of the DNA template during transcription. *Proc. Natl. Acad. Sci. U.S.A.*, **84**, 7024–7027.
83. Ma,J., Bai,L. and Wang,M.D. (2013) Transcription under torsion. *Science*, **340**, 1580–1583.
84. Dame,R.T., Noom,M.C. and Wuite,G.J. (2006) Bacterial chromatin organization by H-NS protein unravelled using dual DNA manipulation. *Nature*, **444**, 387–390.
85. Wiggins,P.A., Dame,R.T., Noom,M.C. and Wuite,G.J. (2009) Protein-mediated molecular bridging: a key mechanism in biopolymer organization. *Biophys. J.*, **97**, 1997–2003.
86. Mayer,O., Rajkowitsch,L., Lorenz,C., Konrat,R. and Schroeder,R. (2007) RNA chaperone activity and RNA-binding properties of the *E. coli* protein StpA. *Nucleic Acids Res.*, **35**, 1257–1269.
87. Park,H.S., Ostberg,Y., Johansson,J., Wagner,E.G. and Uhlin,B.E. (2010) Novel role for a bacterial nucleoid protein in translation of mRNAs with suboptimal ribosome-binding sites. *Genes Dev.*, **24**, 1345–1350.
88. Koster,D.A., Crut,A., Shuman,S., Bjornsti,M.A. and Dekker,N.H. (2010) Cellular strategies for regulating DNA supercoiling: a single-molecule perspective. *Cell*, **142**, 519–530.
89. Rangarajan,A.A. and Schnetz,K. (2018) Interference of transcription across H-NS binding sites and repression by H-NS. *Mol. Microbiol.*, doi:10.1111/mmi.13926.
90. Prosseda,G., Falconi,M., Giangrossi,M., Gualerzi,C.O., Micheli,G. and Colonna,B. (2004) The *virF* promoter in Shigella: more than just a curved DNA stretch. *Mol. Microbiol.*, **51**, 523–537.
91. Lucchini,S., McDermott,P., Thompson,A. and Hinton,J.C. (2009) The H-NS-like protein StpA represses the RpoS (σ38) regulon during exponential growth of *Salmonella Typhimurium*. *Mol. Microbiol.*, **74**, 1169–1186.
92. Nieto,J.M., Carmona,M., Bolland,S., Jubete,Y., de la Cruz,F. and Juárez,A. (1991) The *hha* gene modulates haemolysin expression in *Escherichia coli*. *Mol. Microbiol.*, **5**, 1285–1293.
93. Thomas,S., Holland,I.B. and Schmitt,L. (2014) The type 1 secretion pathway—the hemolysin system and beyond. *Biochim. Biophys. Acta*, **1843**, 1629–1641.
94. Müller,C.M., Dobrindt,U., Nagy,G., Emody,L., Uhlin,B.E. and Hacker,J. (2006) Role of histone-like proteins H-NS and StpA in expression of virulence determinants of uropathogenic *Escherichia coli*. *J. Bacteriol.*, **188**, 5428–5438.
95. Leeds,J.A. and Welch,R.A. (1996) RfaH enhances elongation of *Eschericia coli hlyCABD* mRNA. *J. Bacteriol.*, **178**, 1850–1857.
96. Lim,C.J., Lee,S.Y., Kenney,L.J. and Yan,J. (2012) Nucleoprotein filament formation is the structural basis for bacterial protein H-NS gene silencing. *Sci. Rep.*, **2**, 509.
97. Yun,S.H., Ji,S.C., Jeon,H.J., Wang,X., Lee,Y., Choi,B.S. and Lim,H.M. (2012) A mutational study of Cnu reveals attractive forces between Cnu and H-NS. *Mol. Cells*, **33**, 211–216.
98. Kleckner,N., Fisher,J.K., Stouf,M., White,M.A., Bates,D. and Witz,G. (2014) The bacterial nucleoid: nature, dynamics and sister segregation. *Curr. Opin. Microbiol.*, **22**, 127–137.
99. Shindo,H., Iwaki,T., Ieda,R., Kurumizaka,H., Ueguchi,C., Mizuno,T., Morikawa,S., Nakamura,H. and Kuboniwa,H. (1995) Solution structure of the DNA binding domain of a nucleoid-associated protein, H-NS, from *Escherichia coli*. *FEBS Lett.*, **360**, 125–131.
100. Cordeiro,T.N., Schmidt,H., Madrid,C., Juárez,A., Bernado,P., Griesinger,C., Garcia,J. and Pons,M. (2011) Indirect DNA readout by an H-NS related protein: structure of the DNA complex of the C-terminal domain of Ler. *PLoS Pathog.*, **7**, e1002380.
101. Mahadevan,S. and Wright,A. (1987) A bacterial gene involved in transcription antitermination: regulation at a Rho-independent terminator in the *bgl* operon of *E. coli*. *Cell*, **50**, 485–494.